A Ramachandran Based Analysis to Investigating Amyloids

Samantha Liu[1]

Dr. Amanda Woerman[2]

Departments: Biochemistry and Molecular Biology[1], Biology[2]

Commonwealth Honors College Thesis

University of Massachusetts Amherst - Spring 2021

ABSTRACT

The majority of neurodegenerative diseases (NDDs), including Alzheimer's Disease (AD) and Parkinson's Disease (PD) are caused by protein misfolding. The general mechanism consists of an initial misfolding event of tau and amyloid-ß (AD patients) and α-synuclein (PD patients) to a ß-sheet rich amyloid fibril seed. Following the formation of the misfolded seed, subsequent rounds of templating and propagation of the amyloid fibril leads to aggregate formation and ultimately cell death. Improved structural techniques have enabled the resolution of many amyloid structures, illustrating the diverse amyloid conformations a single protein can adopt, termed strains, with each structure having distinct biochemical and pathological properties evidenced in cellular, mouse, and cell-free studies. While many studies are investigating the process of templating among misfolded proteins, the question of how initial misfolding occurs and how that contributes to strain formation remains unclear. The aim of this study was to survey structures of amyloid proteins deposited in the Protein Data Bank (PDB), an open source repository for three-dimensional nucleic acid and protein structures, and employ a Ramachandran-based analysis to investigate strain formation. The conservation of the dihedral angles phi and psi were analyzed across residues of amyloid structures. Initial analyses revealed the presence of multiple chain redirection/reversal motifs in the α-synuclein amino acid sequence, often forming at consistent residue locations. The presence of extrinsic and intrinsic factors including particular chain redirection/reversals, mutations/post-translational modifications, cofactor presence, and fibril sources were investigated to see how they correlated with dihedral angle variability. Combining these findings, a hierarchy was generated to determine which of the tested factors would have the greatest influence on strain formation, hypothesized as having the lowest dihedral angle variability. There appeared to be little

statistically significant difference between dihedral angles of fibrils with mutations/post-translational modifications and those without, suggesting that factor to perhaps be the least influential on misfolding. The other three comparisons were unable to be ranked due to varying results with phi and psi. The findings will help to elucidate the factors that drive initial strain formation, contributing to an overall better understanding of prion characterization.

ACKNOWLEDGEMENTS

This research did not require any funding.

Dihedral angles were mined using the PDB and MOE software. MOE software was generously provided by Chemical Computing Group.

TABLE OF CONTENTS

LIST OF FIGURES AND TABLES

Supplementary Figures & Tables

LIST OF ABBREVIATIONS

- Alzheimer's Disease (AD)
- Chemical Computing Group (CCG)
- Chronic traumatic encephalopathy (CTE)
- Corticobasal degeneration (CBD)
- Creutzfeldt-Jakob disease (CJD)
- Cryo-electron microscopy (cryo-EM)
- Cryo-electron tomography (cryo-ET)
- Dementia with Lewy Body (DLB)
- Glial cytoplasmic inclusion (GCI)
- Human embryonic kidney 293T (HEK293T)
- Hydrogen-deuterium (HD)
- Lewy Body (LB)
- Micro-electron diffraction (micro-ED)
- Molecular Operating Environment (MOE)
- Multiple System Atrophy (MSA)
- Neurodegenerative diseases (NDDs)
- Non-amyloid ß Component (NAC)
- Olivopontocerebellar atrophy (OPCA)
- Parkinson's Disease (PD)
- Parkinson's Disease with dementia (PDD)
- Phosphotungstic acid (PTA)
- Pick's Disease (PiD)
- Post translational modifications (PTMs)
- Preformed fibril (PFF)
- Prion protein (PrP)
- Prion protein cellular isoform (PrPC)
- Prion protein scrapie isoform (PrPSc)
- Protein Data Bank (PDB)
- Protein misfolding cyclic amplification (PMCA)
- Proteinase K (PK)
- Solid state nuclear magnetic resonance spectroscopy (ssNMR)
- Shy Drager Syndrome (SDS)
- Striatopallidal-nigral degeneration (SND)
- Thioflavin T (ThT)
- Transmission electron microscopy (TEM)
- Yellow fluorescent protein (YFP

INTRODUCTION

Neurodegenerative diseases (NDDs) are a class of diseases involving the dysfunction and loss of neurons, resulting in severe motor/cognitive symptoms and death. Over the years, NDDs have become a growing health concern, especially among aging populations. These diseases are generally classified based on the clinically presenting symptoms, as well as the type(s) of neuropathology observed in patient brains upon autopsy. Although the exact mechanism of many of these diseases remains unknown, various proteins have been identified as playing a key role in the pathogenesis of different NDDs (Dugger and Dickson, 2017). The most prevalent NDDs are Alzheimer's Disease (AD) and Parkinson's Disease (PD), which are caused by misfolding and accumulation of the proteins tau and Aß, and α-synuclein respectively (Martin, 1999). Subsequent templating and propagation of the misfolded conformation among neuronal and glial cells result in the formation of aggregates that ultimately lead to cell death.

The concept of protein misfolding leading to a fatal disease was first proposed by Dr. Stanley Prusiner, describing a proteinaceous infectious particle, termed prion, capable of spreading and propagating disease (Prusiner, 1982). The general mechanism followed by all amyloid forming proteins starts off with the initial misfolded seed formation, whereby the soluble native state protein (such as proteins like tau, or α-synuclein) somehow adopts a misfolded confirmation enriched in ß-sheet content. This change from a generally more α-helical or disordered state to one with more ß-sheets can occur upon exposure to the misfolded protein, such as in prion diseases like bovine spongiform encephalopathy (where transmission through consumption of infected meat is observed) as well as spontaneously among human patients with NDDs. Additional factors such as familial mutations in PD have been observed to increase the propensity of this.

Following initial seed formation, additional monomers of the soluble protein can template off of the misfolded seed, propagating this prion conformation. After repeated rounds of templating, this can result in the formation of aggregates. As evidenced by the structural data published over the last decade, the initial misfolding of the seed can give rise to multiple different conformations, termed strains, as explained by the strain hypothesis (Collinge and Clarke, 2007). PD and multiple system atrophy (MSA) both arise from the misfolding of α-synuclein, however differences between the two diseases (which include contrasting pathological and biochemical characteristics) are attributed to the ability of α-synuclein to adopt multiple different amyloid conformations, a quality observed among other amyloid proteins as well.

While the templating aspect in the second part of the misfolding mechanism of prion diseases has been studied, one of the biggest questions remains: what are the intrinsic and extrinsic factors that drive the initial misfolding of the amyloid forming protein to the misfolded seed, and are some more influential than others? Intrinsic factors such as the presence of mutations associated with familial cases of diseases, as well as post-translational modifications can potentially play a role in the initial seed formation of an amyloid. Extrinsic factors like the presence of a cofactor (Schweighauser *et al.*, 2020) as well as the type of buffer used to generate recombinant fibrils published in structural studies can likewise contribute to strain formation. The degree to which each of these factors have influence on the initial misfolding process remains unclear. The aim of this study is to survey structures of amyloid-forming proteins deposited in the Protein Data Bank (PDB) and employ a Ramachandran-based analysis in order to characterize structural elements among amyloids, as well as analyze the impact of each of these extrinsic and intrinsic factors described above on dihedral angle variability.

Ramachandran plots are scatterplots mapping the phi and psi angles (dihedral angles) of each variable (R) group in a polypeptide chain. These angles represent the orientation of the R group projection relative to the backbone and amino and carboxyl termini of the amino acid, with phi (ϕ) being the torsional angle of the amino group and central alpha-carbon, and psi (Ψ) being the torsional angle of the central alpha-carbon and carbonyl carbon. The ranges for each of the angles span from -180º to 180º (as theoretically the groups can rotate in a full circle about the bond. Data from the Ramachandran plots can be used to infer secondary structural elements (ß-sheets and α-helices) based on the distributions generated (Ramachandran *et al.*, 1963).

Preliminary Ramachandran plots were generated to compare amyloid proteins published in the PDB to their non-amyloid counterparts, looking for potential differences in distribution. Following the generation of these plots, each of the amyloids were analyzed for all of the chain redirections/reversals present in each structure, noting their shape and location along the amino acid sequence in order to categorize them. These findings culminated in conducting a dihedral angle variation comparison across four different categories based upon intrinsic/extrinsic factors within the amyloid proteins in order to identify which particular factors may contribute to a lower phi/psi angle variability across the structures and thus likely play a more influential role in the initial misfolding process. The intrinsic and extrinsic factors analyzed were the fibril source (patient or recombinant), the presence of mutations or post-translational modifications, the presence of a chain redirections/reversals at the 65-70 residue region, and the potential for a small molecule/cofactor. These factors were selected due to their potential in shaping the misfolding pathway of α-synuclein and thus its final conformation. It is hypothesized that the factors that correlate with a lower phi/psi angle standard deviation are more influential in comparison to the other tested factors in the initial misfolding process. The reasoning behind this

is due to the idea that a more conserved phi/psi angle would likely indicate some kind of steric restriction for a particular structure and thus for any factors that correlate with this reduced variability, those factors would likely play a larger role in dictating structure. Building off of this, these conserved regions could potentially be an initial structure or even requisite for successful amyloid formation and templating.

Significance of this Research

As described earlier, the general process followed by protein misfolding diseases consists of the initial misfolded seed formation, whereby the original disordered or soluble state protein adopts an amyloid conformation rich in ß-sheet structures, stabilized by a hydrogen bonding network (Figure 1D). After the initial misfolding, the seed can then serve as a template for subsequent protein monomers to misfold and propagate the amyloid confirmation, ultimately resulting in aggregate formation. While many studies over the years have focused on the propagation process (Woerman *et al.*, 2015; Woerman *et al.*, 2018a; Watts *et al.*, 2013), the key drivers in the initial misfolding process remains unclear. The study aims to address this challenge through the use of phi/psi angle variability to understand the influence of each of these extrinsic and intrinsic factors on amyloid formation.

In recent years, structuctural analysis technology such as cryo-electron microscopy (cryo-EM) and solid state nuclear magnetic resonance spectroscopy (ssNMR) have been greatly improved. This has opened the possibility of capturing and analyzing the structure of various fibrils, especially those isolated from human patient samples. Structural diversity has already been widely observed among the published conformations of amyloid forming proteins. Even among the protein α-synuclein, a variety of elements, including salt-bridges and protofilament

interface interactions are present across amyloids (Li *et al.*, 2018a, Rodriguez *et al.*, 2015, Li *et al.*, 2018b). Differences in these interactions are particularly observed among fibrils generated from recombinant proteins expressing the familial PD mutations H50Q (Boyer *et al.*, 2019) and E46K (Boyer *et al.*, 2020).

Along with structural characterization, Ramachandran plots have been used to characterize secondary structural elements of proteins (Najibi *et al.*, 2017). Previous work analyzing tripeptide residues within various turns have used dihedral angles to differentiate between various ß- and -turns (Venkatachalam, 1968; Némethy and Printz, 1972). These findings demonstrate the possibility of using data extracted from primary sequences to make inferences on overall protein structure, which can be similarly applied to amyloid proteins as well.

Establishing a hierarchy of extrinsic and intrinsic factors that dictate strain formation will hopefully help redefine prions based upon their protein chemistry, and serve as a critical tool in better understanding prion diversity from a structural perspective. Elucidating the impact each of these factors have on fibril formation will contribute to an overall clearer picture of the misfolding mechanisms of prions, and what exactly drives strain formation. Thus the formation of fibrils leading to various different diseases caused by the same amyloid forming protein can be understood mechanistically, and overall how a particular disease arises in order to ultimately develop a treatment plan that targets these mechanisms.

SUMMARY OF WORK OF PREVIOUS RESEARCHERS

A REVIEW ON SYNUCLEINOPATHY STRAINS

While protein misfolding contributing to disease is observed among numerous amyloid forming proteins, this review is focused primarily on α-synuclein due to the availability of structural data. Synucleinopathies are a class of neurodegenerative disorders (NDDs) characterized by the misfolding and spreading of different conformations of the protein α-synuclein, a 140-amino acid intrinsically disordered protein. Although its specific function remains unclear, α-synuclein is thought to be involved in presynaptic signaling by regulating the release of neurotransmitters (Stefanis *et al*., 2012). Previous studies have elucidated the role α-synuclein plays in the SNARE-complex, a protein complex that is required for mediating vesicle interactions at the presynaptic terminal (Burré *et al.*, 2015). Earlier investigations by Burré *et al*. revealed that α-synuclein interacts directly with synaptobrevin-2/VAMP2 within the SNARE complex (Burré *et al.*, 2010), promoting its assembly through the binding and clustering of synaptic vesicles and subsequent fusion of vesicles to the presynaptic membrane (Burré *et al.*, 2015).

Introduction to Synucleinopathies

James Parkinson authored the earliest published case study of PD in, "An essay on the shaking palsy." Parkinson described a disorder observed across multiple patients with common symptoms including weak limbs, convulsions, speech impediment, difficulty chewing food, involuntary excretion/urination, as well the hallmark symptom of an uncontrollable tremor, (Parkinson, 1817). The majority of PD cases occur in individuals fifty years of age and older, and are observed to progressively worsen over time. Interestingly, the onset of motor deficits

occurs asymmetrically in some patients, with one side of the body experiencing more severe motor decline. Such deterioration poses substantial challenges in everyday tasks such as writing, holding utensils for eating, standing, and walking. Speech articulation is also an obstacle among patients, as drooling and a droopiness in facial expression develop. Upon autopsy, swelling within certain areas of the brain is observed, including the medulla oblongata. It was not until the early 1900s that Fritz Jacob Henrich Lewy identified the presence of aggregates, now termed Lewy bodies (LBs), in the neurons of PD patients, which are now recognized as the defining hallmark of PD (Forster and Lewy, 1912).

Around the same time, Dejerine and Thomas published a case study of a patient who had developed the disease olivopontocerebellar atrophy (OPCA). In the report, the authors described the slow progression of a disease with initial symptoms including tiredness and dizziness while walking, difficulty maintaining balance, and tremor (Dejerine and Thomas, 1900). Over time the symptoms progressed to difficulty speaking, jerky movements, and changes in personality. Shy and Drager published a report of a similar NDD characterized by orthostatic hypotension, along with limb rigidity and tremor, which was later named Shy Drager syndrome (SDS) (Shy and Drager, 1960). van der Eecken and colleagues reported a third NDD, termed striatopallidal-nigral degeneration (SND), which exhibited several crossover symptoms with OPCA and SDS (van der Eecken *et al.*, 1960). Initially recognized as separate NDDs, the similarity in clinical symptoms led to the suggestion by Graham and Oppenheimer that the three conditions (OPCA, SDS, and SND) be reclassified under the unifying disorder MSA (Graham and Oppenheimer, 1969). While patients displayed variation in symptoms and lesions, all developed a CNS-targeting neuronal atrophy that led to a progressive degenerative disorder.

Using silver staining techniques on brain and spinal cord samples collected from deceased MSA patients, Papp and Lantos identified the presence of glial cytoplasmic inclusions (GCIs) twenty years after the reclassification of MSA. All MSA patient samples were characterized by wide-spread GCI distribution throughout the putamen, pallidum, lateral caudate nucleus, pons, middle cerebellar peduncle, cerebellar white matter, and spinal cord intermediate grey. This finding established GCIs as the hallmark of MSA neuropathology and reaffirmed the classification of OPCA, SDS, and SND as variants of the same underlying disorder (Papp *et al.* 1989).

In contrast with GCIs in MSA, LBs and Lewy neurites are the pathological hallmark of PD. These lesions are predominantly found in the substantia nigra early in disease, but spread to other brain regions as the disease progresses. Immunostaining of PD patient samples revealed that a major component of LBs is the protein α-synuclein (Spillantini *et al.* 1997). One year later, it was determined that α-synuclein is also a component of GCIs in MSA patient samples. This provided important evidence for the classification of both PD and MSA as synucleinopathies (Spillantini *et al.* 1998).

At the same time Robert Nussbaum and his team conducted a large scale genomic study tracing mutations related to the cases of familial PD among the Contursi kindred in Italy (Polymeropoulos *et al.* 1997). Using a contig constructed from an artificial yeast chromosome aligned to the family DNA sequence, the group identified the gene coding for α-synuclein. The sequencing results revealed a base pair substitution G209A in the fourth exon of the α-synuclein gene (SNCA), resulting in the A53T point mutation. This mutation, which was not present in the non-PD family members, was identified in four additional families with a history of PD, highlighting the critical role of α-synuclein in PD pathogenesis (Polymeropoulos *et al.* 1997).

Structure of α-synuclein

The 140-amino acid sequence of α-synuclein can be categorized into three general domains: the N-terminal domain (residues 1-60), the non-amyloid-ß component (NAC; residues 61-95), and the C-terminal domain (residues 96-140; Figure 1A). Upon binding of the lysine rich N-terminal domain to a lipid or membrane (Bussell and Eliezer, 2003), α-synuclein shifts from its disordered state to one consisting of two antiparallel alpha helices (Elizer, 2001; Ulmer, 2005), while the acidic C-terminal domain remains disordered and free to interact with metal binding partners (Eliezer, 2001; Figure 1B). Upon exposure to a misfolded seed, or through spontaneous means involving factors such as a familial mutation, buffer conditions, or cofactor presence facilitating amyloid formation, α-synuclein shifts from an alpha-helical rich conformation to one high in ß-sheet content, with the NAC region forming the hydrophobic core of the amyloid fibril (Figure 1C, 1D). The N- and C-terminal regions remain disordered, termed the "fuzzy coat" (Tuttle *et al.*, 2016).

Synuclein Prions

In 1982, Dr. Stanley Prusiner first proposed the idea that misfolded proteins are capable of transmitting NDDs, introducing the term 'prion' to describe the 'proteinaceous infectious particle' responsible for scrapie in sheep and goats and Creutzfeldt-Jakob disease (CJD) in humans (Prusiner, 1982). Using a series of experiments to selectively degrade DNA, RNA, and protein, Prusiner demonstrated that the infectious material in scrapie samples is resistant to heat inactivation and nuclease digestion. However, proteinase K (PK) digestion, as well as extraction with stringent chemical denaturants rendered the scrapie agent inactive. Combined, these findings supported the hypothesis that the infectious and transmissible species in scrapie and

CJD is a protein-based particle that develops from the prion protein (PrP). Analysis of brain samples from healthy individuals revealed that only the cellular isoform (PrPC) was present, and was successfully digested by PK. Diseased brains, however, contained a mixture of the PrPC isoform and the scrapie (PrPSc) isoform, which is partially PK-resistant (Basler *et al.*, 1986)

In line with prion disease research and the strain hypothesis, α-synuclein misfolds into distinct disease-causing conformations characterized by unique strain-specific properties that give rise to different synucleinopathies, behaving just like a prion. The earliest pieces of evidence suggesting synucleinopathies exhibit prion behavior arose from neuropathological observations of PD patients who received fetal tissue grafts of dopaminergic neurons as a treatment for neuronal loss (Kordower *et al.*, 1995). While the treatments were ultimately unable to extend lifespan, patients that lived more than ten years after receiving tissue transplants developed LB pathology that spread from the host to the grafted tissue (Li *et al.*, 2008; Kordower *et al.*, 2008), demonstrating that α-synuclein can propagate intracellularly, similar to PrPSc.

The ability of α-synuclein to form aggregates in both PD and MSA patients has also raised the question of how α-synuclein gives rise to discrete diseases and neuropathologies, a phenomenon observed among other protein misfolding disorders. To explain this observation, the strain hypothesis was introduced, proposing that different conformations, or strains, of misfolded PrP give rise to different diseases (Collinge and Clarke, 2007).

The Strain Hypothesis of Synucleinopathies

Like PrP, α-synuclein has the ability to misfold into multiple different amyloid conformations. More recently, structurally-focused methods have been used to characterize and define distinct α-synuclein strains in PD and MSA. New cryo-electron microscopy (cryo-EM)

data of samples isolated from patients with confirmed cases of MSA revealed two types of filament structures, denoted as Type I and Type II MSA conformations. Each structure is composed of asymmetrical protofilaments, with three positively charged residues (K43, K45, and H50) surrounding a non-proteinaceous molecule (Schweighauser *et al.*, 2020). To date, no structures have been successfully isolated from PD patient samples. Protein misfolding cyclic amplification (PMCA), which uses serial rounds of shaking and sonication to facilitate amplification of misfolded proteins, is a technique that was first developed to investigate PrPSc strains in vitro. Recently, multiple groups have adapted PMCA to amplify and characterize α-synuclein strains, as well. Transmission electron microscopy (TEM) analysis of PMCA amplified PD- and MSA-derived fibrils revealed that both contain a twisted and flat ribbon structure, however, a related disease, dementia with Lewy bodies (DLB), induced cylindrical fibrils. These structural differences are consistent with the variation in PK digestion results observed across the three patient samples (Van der Parren *et al.*, 2020).

Analysis of aggregate formation among PMCA amplified PD and MSA samples has also revealed differences in maximum emission and overall absorption spectra based on thioflavin T (ThT) fluorescence, a conformational dependent amyloid binding dye (Shahnawaz *et al.*, 2020). Structural analysis studies conducted using circular dichroism and FTIR spectroscopy techniques revealed the prevalence of ß-sheet rich structures in both PD- and MSA-derived patient samples. However, cryo-electron tomography (cryo-ET) analysis revealed differences in fibril twist length between the two samples, suggesting a more tightly coiled structure among MSA α-synuclein aggregates than PD derived aggregates (Shahnawaz *et al.*, 2020). These findings are in agreement with previously published data using hydrogen-deuterium (HD) exchange and changes in emission spectra following incubation of the amyloid-binding dye curcumin with

PMCA-amplified α-synuclein aggregates isolated from PD and MSA patient samples (Strohäker *et al.*, 2019). Altogether, these analyses provide compelling evidence that structural diversity among α-synuclein fibrils likely contributes to biochemical and clinical differences among PD, DLB, and MSA patients (Strohäker *et al.*, 2019).

Development of Strain-Specific Cellular Assays

Several cell-based models exist to investigate α-synuclein misfolding and propagation in disease. The most frequently used cell model is human embryonic kidney 293T (HEK293T) cells, which express human α-synuclein containing the A53T mutation with a C-terminal yellow fluorescent protein (YFP) tag (α-syn140*A53T-YFP cells; Woerman *et al.*, 2015). Under normal culture conditions, α-synuclein is distributed throughout the cytoplasm of the cell, as visualized by the YFP tag via live-cell microscopy. In the presence of α-synuclein prions isolated from MSA patient samples via phosphotungstic acid (PTA) precipitation, the cells develop bright yellow puncta (Woerman *et al.*, 2015). Interestingly, while PD, PD with dementia (PDD), and DLB patient samples contain similar concentrations of α-synuclein as MSA samples, they are unable to propagate in the α-syn140*A53T-YFP cells, which could be explained by the hypothesis that distinct α-synuclein strains give rise to MSA and PD. Other studies have also reported variations in the toxic effects caused by infection with different patient samples. Primary oligodendrocytes expressing α-synuclein-mCherry infected with α-synuclein aggregates derived from GCIs of MSA, LBs of PD patients, or preformed fibrils (PFFs) made from recombinant protein revealed that MSA-infected cells had nearly 1000 times more pathogenic α-synuclein than LB- or PFF-infected cells (Peng *et al.*, 2018). These results suggest the difference in aggregate potency arises due to distinct strains.

To further investigate the strain differences between PD and MSA, a panel of cell lines expressing various PD familial mutations was created to test the effect of other PD-causing mutations on MSA prion propagation *in vitro*. While the MSA samples were able to propagate in cells expressing WT α-synuclein or the A30P mutation, the E46K mutation, which was identified in a Basque Country patient cohort of confirmed DLB cases (Zarranz *et al.*, 2004), blocked MSA infection (Woerman *et al.*, 2018a). Co-expression of the A53T and E46K mutations was unable to rescue the inhibitory effect of the E46K mutation on MSA infection (Woerman *et al.*, 2018a), demonstrating that the misfolded α-synuclein conformation in MSA must be distinct from the conformation in E46K patients.

This result is supported by the recently published cryo-electron microscopy (cryo-EM) structures of misfolded α-synuclein isolated from MSA patient samples (Schweighauser *et al.*, 2020). In all three structures, a salt bridge between the glutamic acid at residue 46 and the lysine at residue 80 stabilizes the "central" and "outer" layers of each protofilament, forming the characteristic Greek key motif (Schweighauser *et al.*, 2020). Consequently, the E46K mutation would produce a charge-charge repulsion with residue K80 that would likely destabilize this fold, indicating a structural incompatibility between the E46K mutation and the published MSA conformations.

Evidence of Multiple α-Synuclein Strains in Mouse Models

In addition to cell models, animal models have been used to study transmission of α-synuclein. The most commonly used transgenic mouse model of synucleinopathy is the TgM83 mouse, which uses the mouse prion promoter to express human α-synuclein with the A53T mutation (Giasson *et al.*, 2002). Homozygous TgM83$^{+/+}$ mice spontaneously develop weight

loss, reduced grooming, decline in ambulation, freezing of hindlimbs, limb paralysis (progressing from hind to forelimbs), passive movement resistance, tremors, back hunching, inability to stand upright, and difficulty feeding as early as 8 months of age (Watts *et al.*, 2013). Initial studies investigating α-synuclein transmissibility used brain homogenates obtained from symptomatic 12-18 month old homozygous TgM83$^{+/+}$ mice to inoculate 7-9 week old TgM83$^{+/+}$ mice (Mougenot *et al.*, 2011). This resulted in accelerated disease onset and death in the infected mice, as well as formation of hyperphosphorylated (pS129) α-synuclein aggregates (Mougenot *et al.*, 2011, Luk *et al.*, 2012). Inoculation of PFFs into young M83 mice also led to hyperphosphorylated α-synuclein inclusions spreading from the injection site along major axonal pathways, demonstrating the ability of α-synuclein to propagate *in vivo* (Luk *et al.*, 2012).

As the TgM83$^{+/+}$ mice develop spontaneous disease, one criticism of these studies is that the inoculations could simply be accelerating disease onset, rather than demonstrating transmissibility. Notably, the hemizygous TgM83$^{+/-}$ mice do not spontaneously develop neurological signs or pathological α-synuclein inclusions within 600 days (Watts *et al.*, 2013). However, inoculation of α-synuclein isolated from MSA or TgM83$^{+/+}$ mouse samples into the hemizygous mice induces motor deficits and detergent-insoluble hyperphosphorylated α-synuclein aggregates, supporting the initial conclusions that misfolded α-synuclein transmits disease, similar to PrP prions, rather than simply accelerating disease progression (Watts *et al.*, 2013). Importantly, TgM83$^{+/-}$ mice infected with TgM83$^{+/+}$ prions develop deficits ~180 days post inoculation (dpi), while mice infected with MSA prions develop symptoms ~120 dpi (Watts *et al.*, 2013). The different incubation times between the two prion sources, likely characterized by unique biochemical properties, suggests they are two distinct strains.

In contrast, inoculation studies using PD patient samples failed to transmit disease to the TgM83$^{+/-}$ mice (Prusiner *et al.*, 2015). In unpublished experiments, MSA inoculations in mice expressing the familial PD E46K mutation (TgM47$^{+/-}$ mice) did not transmit disease, whereas PFFs expressing the E46K mutation induced neurological symptoms in the animals. These findings are consistent with the cell culture studies and cryo-EM structures (Schweighauser *et al.*, 2020) previously discussed.

Additional studies investigating α-synuclein strain biology in the TgM83 mice were recently published by Joel Watts' group (Lau *et al.*, 2020). PFFs were prepared in either salt (S) or no salt (NS) conditions to generate two distinct fibril strains with unique conformations and biochemical properties. The S and NS fibrils induced two different incubation periods after inoculation in TgM83 mice, resulting in different clinical presentations and inclusion distributions. These findings were in line with differences also observed among mice inoculated with either TgM83$^{+/+}$ or MSA brain homogenates (Watts *et al.*, 2013, Lau *et al.*, 2020), and were maintained throughout a second and third passage, establishing strong support for the hypothesis that specific disease characteristics are encoded by prion strain rather than the host organism (Lau *et al.*, 2020).

Structural Variation Among α-Synuclein Amyloids

In general, amyloid structures consist of repetitive protofilaments rich in ß-sheets that stack into layers along the fibril axis (with each polypeptide perpendicular to the fibril axis), stabilized by hydrogen bonding between the residues (Eisenberg and Jucker, 2012). Additional characteristic features of amyloids include in-register alignment, as well as the ability to form parallel structures (Eisenberg and Jucker, 2012). Several α-synuclein amyloid structures have

been reported using various fibril sources and imaging methods, which are discussed in detail below.

Micro-electron diffraction (micro-ED) was used to resolve the structure of 11-residue crystals of the non-amyloid ß component (NAC) core of α-synuclein, which is known to play a significant role in the aggregation and toxicity of the protein (Rodriguez *et al.*, 2015). Structural analysis revealed that these short segments form steric zipper structures, with X-ray diffraction patterns comparable to those of full length α-synuclein polymorphs (Rodriguez *et al.*, 2015). In 2016, the first solid state nuclear magnetic resonance (ssNMR) structure of recombinant full-length human α-synuclein revealed a Greek-key motif within the fibril core (Tuttle *et al.*, 2016), which has remained a characteristic feature in subsequent α-synuclein structures. Several notable interactions stabilize the structure, including the salt bridge between residues E46 and K80, a hydrophobic core with residues I88, A91, and F94, and hydrogen bonding networks between ß-sheets, and steric zippers. More recently, numerous cryo-EM studies have reported common morphological characteristics of stacked ß-sheet rich structures with the characteristic bent ß-arch and Greek key motifs revealed in the original ssNMR structure (Guerrero-Ferreira *et al.*, 2018, Li *et al.*, 2018a, Li *et al.*, 2018b). Fibril structure can also vary greatly, with differences in overall shape, pitch, twist, number of protofilaments, and filament diameter (Guerrero-Ferreira *et al.*, 2019). In contrast to the ssNMR structure, the cryo-EM structures of α-synuclein fibrils contain two stacked filaments, instead of a single protofilament, with residues 38-95 forming the templating region, as well as an interface region between the two protofilaments (Guerrero-Ferreira *et al.*, 2018). These cryo-EM structures for both WT and mutant α-synuclein also generally contain a hydrophobic core flanked by hydrophilic segments termed the “fuzzy coat”

region, which is more disordered, similar to the ssNMR structure (Guerrero-Ferreira *et al.*, 2018, Tuttle *et al.*, 2016).

Among the various polymorphs of α-synuclein, differences in the steric zipper interactions between the protofilament faces exist across structures. In a structural analysis by Li *et al.* 2018a, two general populations of full-length human α-synuclein recombinant polymorphs were observed, termed the rod and twister species (Li *et al.*, 2018a). Both structures contained the characteristic ß-arch and Greek-Key motif in the symmetric protofilaments, however the steric interface in the rod polymorph occurred within the preNAC region of α-synuclein (residues 47-56), while the twister polymorph protofilament interface involved the NACore region (residues 68-78) (Li *et al.*, 2018a, Rodriguez *et al.*, 2015). Six familial PD mutations are located within the preNAC region (E46K, H50Q, G51D, A53E, A53T, A53V), which would likely disrupt the steric zipper interaction between the protofilaments of the rod species. In contrast, the exclusion of the preNAC region at the steric interface of the twister protofilaments reduces the effect these mutations would have on the structural integrity of twister fibrils (Li *et al.*, 2018a).

Similar findings have been observed among other published cryo-EM structures as well, with one recombinant full length α-synuclein structure forming a steric interface between its two protofilaments at residues 50-57 (Li *et al.*, 2018b). Mutations G51D and A53T/E lead to the substitution of a hydrophilic residue within the hydrophobic interface, while the H50Q mutation disrupts electrostatic interactions with residue E57. As previously mentioned, the E46K mutation disrupts the salt bridge formed with K80, which stabilizes the ß-arch structure (Li *et al.*, 2018b). Thus the presence of familial PD mutations have been hypothesized to disrupt the WT conformations of α-synuclein. It has since been proposed that fibrils with these mutations adopt alternate conformations that promote aggregate formation, leading to increased toxicity. In

published structures of α-synuclein fibrils with the H50Q mutation, two new polymorphs were revealed: a narrow fibril containing one protofilament, and a wide fibril containing two protofilaments. Both fibrils have overall folding structures similar to the WT fibril (Boyer *et al.*, 2019), however, the H50Q mutation contributes to a structure containing a smaller protofilament interface with a steric zipper outside of the NACore and preNAC regions (Boyer *et al.*, 2019). In several WT α-synuclein fibril structures, residue H50 forms a salt bridge with residue E58 which stabilizes the steric zipper. The glutamine mutation disrupts this interaction, impacting the stability of the interface interactions (Li *et al.*, 2018a) or shifting intramolecular bonding (Boyer *et al.*, 2019).

A key observation shared among the published cryo-EM structures of recombinant and patient fibrils is the presence of an unknown molecule in the core of the filaments. Positively charged residues (K43, K45, H50) can be observed surrounding a cavity located between the two protofilaments of the fibril structure (Schweighauser *et al.*, 2020), with the addition of K58 flanking this region among the recombinant fibrils (Guerrero-Ferreira *et al.*, 2018). It is postulated that a non-proteinaceous molecule, likely negatively charged, resides within this region, offering stability to the overall filament structure (Guerrero-Ferreira *et al.*, 2018).

Modeling Protein Misfolding

The importance of misfolded protein structure in prion diseases has led to considerable research on the dynamics and interactions of protein misfolding. Multiple studies have developed modelling techniques to predict folding activity and changes that may occur as a consequence of a mutation. Christopher M. Dobson's team developed a mathematical model that predicts the aggregation propensity of different amyloids, as well as globular proteins that have the potential

to form aggregates, based on the primary structure of the polypeptide. Taking several factors into account, including hydrophobicity and the potential to form ß-sheets or α-helices, the team was able to construct aggregation propensity profiles by analyzing each amino acid in the polypeptide sequence and predicting aggregation-prone regions (Pawar *et al.*, 2005; Tartaglia *et al.*, 2008). Analysis of α-synuclein using this model predicted that residues 34-97 have a higher aggregation propensity, which corresponds to the templating region of α-synuclein prions (Pawar *et al.*, 2005).

Some of these models, such as the AGGRESCANS3D (A3D) model, are available for public use (Zambrano *et al.*, 2015). Unlike many other models that use a purely linear approach to determining aggregation propensity, A3D accounts for exposed soluble/insoluble regions in the folded structure to determine whether or not a certain sequence is capable of forming aggregates. In addition, it is important to classify types of protein structures, preferably in a quantitative manner, which has long been a challenge for protein modeling. Many groups have designed servers that can classify proteins based on their structure, including FSSP, CATH, and SCOP, by comparing secondary structure and shape of the protein surface; however, as these servers base their classification on visual observation, qualitative elements are introduced (Getz *et al.*, 2004).

One quantitative approach to analyze protein structures utilizes the Ramachandran plot, which is a scatterplot of the dihedral angles along the peptide backbone designated as phi ( ) and psi ( ) (Najibi *et al.*, 2017). These plots can be used to characterize secondary structural elements, such as α-helices and ß-sheets based on the allowable dihedral angles for each amino acid. Ramachandran plots across the twenty amino acids vary due to differences in structure and chemistry of the individual R groups (Hovmöller *et al.*, 2002). Dihedral angle measurements

have also been employed to characterize different ß- and -turns, with certain allowable angles for each of the tripeptide residues comprising each structure (Venkatachalam, 1968; Némethy and Printz, 1972). This approach can be applied to amyloid forming proteins as well, to model and describe structural similarities among known prion structures in a quantitative manner.

Conclusion

Critical advancements in the prion and NDD fields have been made in the past two decades. Structural, cellular, and animal studies have revealed the diverse conformations and biochemical characteristics of α-synuclein strains, adding to the evidence of the existence of multiple strains described by the strain hypothesis of the prion field. Despite this growing data on the variety of strains that can exist, little is known about the mechanisms of strain formation and the specific factors that drive the initial misfolding process. Factors such as familial mutation, buffer composition, fibril source, as well as the presence of a cofactor have been thought to influence the conformation of the α-synuclein amyloid, however the degree of impact each of these variables have in comparison to one another remains unclear, demonstrating a need for further investigation on the intrinsic and extrinsic factors that drive strain formation.

COVID-19 Impact Statement

Due to the ongoing COVID-19 pandemic, the nature of this thesis project was completely altered from the original plan prior to Spring 2020. In the absence of COVID-19, the original thesis project aimed at further developing a cell-based assay to be used to discriminate between different strains of α-synuclein amyloids. Due to possible risk of campus-wide closures during this time, a new fully remote project was designed aimed at utilizing data extracted from

published amyloid structures in order to analyze potential relationships between dihedral angle data and amyloid structure. This involved delving into an area of research new to the lab, in addition to learning a new background and software to be able to characterize structures of amyloids published in the PDB.

METHODS

Mining PDB

The Protein Data Bank (PDB) is a public web-based repository filled with published protein structures solved using a variety of structural techniques including but not limited to X-ray crystallography, NMR, and cryo-EM. All amyloid structures published in the PDB were mined, noting characteristics such as fibril source, presence of mutations, length of templating region, method used, resolution, and if they were involved in any diseases (among others). This information was compiled into a spreadsheet, sorting by amyloid protein type. In general, amyloids were defined as structures that were rich in ß-sheets and formed filamentous stacks. Notably the PDB also contained small peptides that were fragments of amyloid forming proteins, which were omitted from the structural analyses due to their short length.

In addition, the globular "counterparts" were mined from PDB, however it is important to note that many of the amyloid forming proteins did not have a non-amyloid counterpart, or were intrinsically disordered proteins (such as α-synuclein) that only had structures bound to another molecule. In the case of α-synuclein this included α-synuclein bound to a micelle in its soluble state (non-amyloid form).

Extracting Phi/Psi Angles and Generating Preliminary Ramachandran Plots

Each amyloid structure was loaded into PyMol software, a molecular visualization tool, and using the phi_psi command, the dihedral angles of all of the residues were extracted (excluding the terminal residues as those by definition do not have phi/psi angles). Preliminary Ramachandran Plots were generated by making scatter plots of the phi and psi angles for each of the 20 amino acids to see if they followed the same distribution as those obtained from globular

proteins. Ramachandran plots were also generated using the Molecular Operating Environment (MOE) software, which is another molecular visualization and analysis tool. Notably however, plots of only glycine, proline, and general amino acid residues could be generated using MOE, so plots of other amino acid residues were generated by making scatter plots manually. Several of the published amyloid structures in the PDB include short 6-11 residue segments. For the purpose of the subsequent analyses, these structures were omitted as they did not contain any chain redirections/reversals motifs, and likely could not provide enough information to the questions being asked in this study.

Categorizing Chain Redirections and Reversals Among Amyloids

Upon mining of the structures deposited in the PDB, chain redirections/reversals motifs in the amyloid structures were particularly characteristic. To further investigate these elements, amyloid structures were analyzed for the presence of chain redirections/reversals, noting the residues that comprise a particular chain redirections/reversals, and where within the chain redirections/reversals they were located (at the point/vertex, or before/after by a certain number of residues, as well as if the structure was left or right handed). For the purpose of this investigation, a chain reversal is defined as a bend in the backbone of the polypeptide sequence, resulting in an antiparallel interaction of the main chain (about 180º), while a chain redirection is a less than 180º orientation of this and closer to 90º. Two general classifications of turns for typical proteins utilizing dihedral angle measurements have been previously defined by Venkatachalam (1968), Richardson (1981), and Némethy & Printz (1972): ß-turns and -turns. In general, a ß-turn is defined by four consecutive residues (designated as i, i+1, i+2, 1+3 where i is the first residue in the turn), with a distance smaller than 7Å between the alpha carbon if i and

i+3. -turns are defined as three consecutive residues (designated as i, i+1, i+2, 1+3 where i is the first residue in the turn), with a hydrogen bond stabilizing residues i and i+2 (Hutchinson & Thornton, 1996). The ß-turns and -turns are further sub classified into specific turn types based on specific ranges of phi/psi angles for each turn (Table I).

Utilizing the PROMOTIF Turn Predictor program (Hutchinson & Thornton, 1996), α-synuclein amyloids were loaded into the PROMOTIF software on the JPred4 site (Drozdetskiy *et al.* 2015) in order to determine if chain redirections/reversals motifs could be detected and obey the predefined turn classification system. While the program appeared to detect some of the chain redirections in the MSA structures published and classify them based on the defined phi/psi angles, many of the chain redirections/reversals were classified as a Type IV ß-turn, which includes all turns that did not fall under any of the other definitions and thus were outliers. In addition, some of the chain redirections/reversals motifs visually detected on the structures were not picked up by the program either, demonstrating a need for a separate classification specific to amyloids like α-synuclein.

Using visual observations, the geometry of the chain redirections/reversals was noted based on a new designed criteria. The first aspect was splitting the chain redirections/reversals by symmetry based on the two protofilaments involved in the overall amyloid structure. For structures that only had one protofilament this was indicated instead of a “symmetrical” or “asymmetrical” designation. Following sorting of the structures based on symmetry, the chain reversals were categorized by their shape into different classifications. Notably, a residue often observed in these chain redirections/reversals motifs were glycines. The location of glycine residues in each chain redirection was plotted by structure type for both α-synuclein and tau amyloids.

Analyzing the Impact of Extrinsic and Intrinsic Factors on Phi/Psi Variability

Considering the presence of chain redirections/reversals motifs across these amyloid structures, this raised the question regarding the variability in the dihedral angle measurements across these amyloids, and if there were particular factors that could potentially contribute to more or less variability in the phi/psi angle distribution. The standard deviation of the dihedral angles for all a-synuclein structures were calculated for each residue. To determine which intrinsic and extrinsic factors have the greatest impact on strain formation, F test (Levene's Test) was used to compare the difference in phi and psi variability across structures. With this analysis, I compared differences in standard deviation between patient vs. recombinant/synthetic fibril, the presence or absence of a small molecule or cofactor, presence of either a chain redirections or reversals at the 65-70 residue region, as well as the presence of a mutation or post-translational modification on phi/psi variability. This approach was used to stratify factors from strongest to weakest influence on strain, as determined by a decrease in dihedral angle variability. I used these findings to generate a hierarchy for how each factor influences strain formation. With the data generated from the published α-synuclein structures, a protein misfolding hierarchy was created to rank the effects of each of these variables on the adoption of an amyloid conformation starting from the disordered/soluble state.

RESULTS AND DISCUSSION

Results

The Role of Glycines in Amyloid Structures

When considering the distribution of points on a Ramachandran plot, one of the most notable residues that occupies the largest space on the chart are glycines. The lack of an R group (since glycines have two hydrogens attached to the alpha carbon), reduces steric hindrance, resulting in a wider range of allowable conformations and thus greater variance in phi/psi occupancy. In general, glycines make up 12.86% of the 140-amino acid long α-synuclein protein sequence, and 10.82% of the 758-amino acid long isoform PNS-tau protein sequence. Focusing on the Ramachandran distributions for α-synuclein, the amyloid structures appear to occupy a larger region on the plot than the globular α-synuclein structures mined from the PDB. Notably, there are a lot fewer globular structures available (21 amyloid compared to 2 globular structures for α-synuclein), which does limit this interpretation. Comparing the α-synuclein amyloid plot to the general Ramachandran plot published for glycines from general globular proteins, there appears to be a higher occupancy particularly in the upper right quadrant among glycines from the amyloid structures (Figure 2). This widespread distribution of glycine residues was also observed among other amyloid forming proteins as well including tau, amyloid-ß, TDP-43, prion protein, and HET-s during initial Ramachandran analyses. The flexibility afforded by the hydrogen residue likely contributes to the wider distribution among the glycine residues and thus a greater number of conformations that it can adopt compared to other residues. Considering the flexibility of glycines, the presence of chain redirections/reversals commonly observed across amyloid structures were analyzed in relation to the presence of glycine residues. In this investigation, the term “chain redirection” generally referred to any bending or curvature of the

protein backbone that was closer to around a 90º angle, while “chain redirection” referred to a change in backbone directionality resulting in a 180º curve and antiparallel strand interactions. We looked at the percentage of chain redirections/reversals with glycine residues in α-synuclein amyloid structures (Table II). For both chain redirections and reversals, the majority of these motifs contained at least one glycine residue.

Among the chain redirections that included a glycine, the location of glycine within chain redirections was then analyzed, with the goal of determining whether or not there was a preference as to where in a chain redirection glycine residues tended to reside. This was done by sorting the locations within a chain redirection as before the vertex, at the vertex, or after the vertex, with the vertex being defined as the convex point of a chain redirection. Going through each of the tau and α-synuclein amyloid structures, the location of the glycines within a chain redirection was marked, and tallied below. Recognizing the differences in fibril source, the data was additionally split by recombinant and patient derived fibril to see if differences in the fibril source would perhaps alter the placement of a glycine residue along the amyloid protein sequence (Figure 3). Among chain redirections with glycines for α-synuclein amyloid structures, the majority of glycines within these chain redirections were located at the vertex position of the chain redirections, at an over 50% among all α-synuclein amyloid structures (Figure 3A). Splitting the structures by fibril source (recombinant and patient derived), the recombinant α-synuclein fibrils follow a similar distribution with a little under 50% of glycines falling at the vertex position (Figure 3B). The patient derived α-synuclein fibrils however are much heavily shifted towards having glycines being located at the vertex of the chain redirections (Figure 3C).

Interestingly, tau amyloid structures appear to show the opposite in terms of comparing recombinant versus patient derived fibrils, whereby the recombinant fibrils have a much greater

population of glycines located at the vertex position (Figure 3E) than the patient derived fibrils (Figure 3F), which show a distribution much more similar to that of all of the tau amyloids in general (Figure 3D). While this distribution is different between α-synuclein and tau, the shift observed with fibril source (patient-derived versus recombinant/synthetic fibrils) provides further evidence that fibril source impacts strain formation. As the location of glycines appear to be skewed towards certain areas of a chain redirection, correlated with the fibril source, this could potentially influence the type of chain redirection able to form, considering the flexibility offered by a glycine residue as observed earlier (Figure 2A).

In addition to chain redirections, the presence of chain reversals contribute to an additional element of structural diversity observed across amyloids. Chain reversals, generally defined in this paper, refer to the inversion of the main polypeptide chain, so that the backbone bends 180º, resulting in two antiparallel strands. As aforementioned, there exists classical turn definitions which utilize the dihedral angle measurements to subcategorize ß- and -turns. Utilizing the PROMOTIF program, which detects and categorizes turns in proteins loaded onto the software, it appears that not all of the chain redirections/reversals are detected, and if they were, they were categorized as Type IV, which was designated as a classification for turns that did not fall into any of the other categories (Table I). In the example shown below, the MSA II Type I filament was loaded onto JPred4 (a site that includes multiple structural analysis softwares), and the PROMOTIF program was run (Figure 4). Analyzing a single chain from each of the two asymmetrical filaments that make up this amyloid, the detected chain redirections are denoted by corresponding color coding. Notably, while several chain redirections are detected by the program, four chain redirections on each of the filaments are classified as Type IV beta turns. Additionally, several of the chain redirections were not detected by the program (areas of the

structure not highlighted/without residues shown in Figure 4). These results suggest that perhaps the chain redirections/reversals observed among amyloids don't fall under the classical definitions for these structural motifs. Given this output, we went through the chain redirections/reversals of the amyloid structures extracted from the PDB and came up with our own classification system based on visual observations.

New Chain Redirections/Reversals Classifications Among Amyloids

For this analysis, chain reversals were focused on instead of chain redirections, due to the greater structural diversity among chain reversals. Going through the length of each amyloid protein mined from the PDB, the location and geometry of the chain reversals were noted. Starting off with symmetry, chain reversals were designated as either symmetrical or asymmetrical, and then sub categorized based on their features. Chain redirections/reversals were noted across all of the amyloid structures. Shown in the figure below are example chain reversal types observed among α-synuclein amyloids (Figure 5). From these definitions, ongoing collaborations with Chemical Computing Group (CCG) are aimed at translating these working criteria into a tool for chain redirections/reversals analysis among amyloids and hopefully build a stronger definition specific to prions. From these findings, a better understanding of these structural motifs and their contributions to strains can be obtained.

Conserved Chain Redirections/Reversals Regions Among Tau and α-synuclein Amyloids

Chain reversal motifs appear to be a great contributor to amyloid structural diversity, with the presence of these motifs. Beyond the shape of the chain reversals contributing to variation in amyloids, the number and location of chain reversals appeared to differ across structures of the

same protein. This raised the question of whether or not there were particular regions of the protein sequence that consistently formed chain redirections/reversals motifs, and if so, whether or not they were observed perhaps in combination with other chain redirections/reversals domains. It was hypothesized that chain reversals that consistently formed at a particular region of residues within an amyloid protein could perhaps be conferring some level of stability to the overall fibril structure. Thinking of the overall misfolding process, these conserved regions could potentially be forming an initial step during the actual mechanism to achieve the final amyloid structure. Following categorization of the chain reversals, the placement and location of the chain redirections/reversals, as well as the combination of chain redirections/reversals observed in each of the structures (this was done for α-synuclein and tau) was analyzed (Figure 6). Among α-synuclein amyloids, the first major chain reversal combinations included chain reversals at residues 65-70 and 80-88 (note there are some variations in chain reversal locations across the structures by a few residues). In addition, structures with chain reversals at these two residue locations also have a chain redirection at residues 72-76 as well. Another chain reversal combination that was observed across multiple structures was at residues 56-61 and 72-76 (except for the Y39 phosphorylated fibrils). Notably, these five structures were also the only structures that did not contain a chain reversal at the conserved residue 65-70 region, but instead, all had a chain redirection. Four of these structures came from the same publication, raising the question of how much of a role the preparation protocol for these recombinant fibrils influenced structure formation, however one of the structures (6UFR) came from a separate publication. The 65-70 chain reversal is also conserved in the three MSA patient samples (also have the 83-88 chain reversal, as well as 19-26 or 32-38 depending on which filament as they are asymmetrical). Looking at the Y39 phosphorylated fibrils (6L1T and 6L1U), these contain the 16-22, 56-62, and

65-71 chain reversals. This could suggest that phosphorylation could change the folding pattern of the amyloid, as they do not contain the 72-76 chain reversal for example despite also containing the 56-62 chain reversal, deviating from the second chain reversal combination described above.

The Influence of Extrinsic and Intrinsic Factors on Phi/Psi Angle Variability

Tying together all of the various observations made across amyloid (and their non-amyloid counterparts), the aim of this investigation was to utilize these findings to build a hierarchy that ranks factors and their influence in the protein misfolding pathway starting from the disordered or soluble state of the protein. After averaging the phi/psi values for each of the residues along the length of identical filaments (separating them as described in the materials & methods section if they were asymmetrical filaments), the standard deviation was taken across each of the average values and plotted against the residue number for the full length of the proteins. This process was done for all α-synuclein and tau amyloids. The goal of this part of the project was to determine if particular fibril comparisons could correlate with a reduction in dihedral angle variability, which would be quantified across all fibril structures of that particular category using standard deviation as a measurement.

The exclusion criterias selected were: fibril source (patient vs. recombinant/synthetic), the presence (or absence) of mutations and/or post translational modifications (PTMs), the potential for a cofactor, and the presence of a chain redirections/reversals at the previously identified 65-70 residue region. Recombinant fibrils included all structures that were synthetically produced, while the patient derived firbils included the 3 MSA structures (as those are the only ones currently available among α-synuclein amyloids). The second comparison

looks at the structures that have either a mutation or PTM in contrast to structures with neither. These mutations/PTMs include E46K, H50Q, A53T, and a phosphorylated T39 residue. Based on previous analyses, the impact of having a chain reversal compared to a chain redirection at the 65-70 residue region was also compared to test the impact of these two structures on dihedral angle variance, considering the observation that the majority of the published structures contain a chain reversal instead of a chain redirection at that location. The fourth category compares the presence, absence, as well as potential of a small molecule at the interface of the fibrils. Of the structures obtained, only the three MSA structures are confirmed to contain a non-proteinaceous cofactor at the protofilament interface, however three recombinant structures appear to have a cavity at the interface region, despite not being explicitly described as having a molecule in that region, instead of a flat interface observed among the rest of the recombinant fibrils. As the involvement of a cofactor appears to be quite important for strain formation especially when considering differences in fibril source, its relationship with phi/psi angle variability was tested.

Differences in variability of dihedral angle measurements across α-synuclein fibrils were analyzed by plotting the standard deviation across filaments (asymmetrical filaments were separated and treated as individual structures in order to best capture their own set of dihedral angles) against the corresponding residue number (Figure 7). Looking at dihedral angle variation across all α-synuclein amyloids, there does appear to be regions of alternating lower and higher variability. Many of the highest standard deviations appear to come from psi angle variability, however upon conducting a Levene's test on the standard deviation between phi and psi angles of all α-synuclein amyloids, there was no statistically significant difference between the two angles ($p = 0.239951219$; $p^* = 0.05$).

Focusing on the comparison between recombinant vs, patient derived α-synuclein structures, the recombinant and general plot are nearly identical (Figures 7, 8A), while the patient structures had reduced variability among both phi and psi angle measurements (Figure 8B). Splitting all of the α-synuclein amyloids by structures without mutations or PTMs and those with either/or resulted in a lower variance in general for structures with mutations or PTMs (Figure 9). This could tie with the hypothesis (described in Boyer *et al.* 2019 as well) that perhaps the introduction of a mutation or PTM would disrupt certain key interactions that facilitate structure formation for specific conformations, and by doing so, reduces the pool of possible conformations that amino acid sequence can adopt. Similarly, the introduction of a small molecule (or potential for one) also appeared to reduce variation across the residues for α-synuclein amyloids, with lower standard deviation values and peaks in general among those categories compared to α-synuclein classified as not having any small molecules (Figure 10). Looking at the presence of a chain redirections/reversals at residues 65-70 in particular, comparison of structures with a chain reversal at this location compared to ones with a chain redirection reveal that there is a lower standard deviation across the residues for structures with a chain redirection at this location (Figure 11). Once again however, four of the five structures in the chain redirection category came from the same publication, highlighting a limitation with this comparison.

To quantify the standard deviation in the comparisons in order to determine which factors may potentially contribute more to strain formation, a Levene's Test was conducted to analyze the differences in variance. Sorting the fibrils into the four aforementioned comparisons, the analysis was performed ($p^* = 0.05$) for variance across angles phi and psi, and the percentages above and below the p value were calculated (Table III). Notably the comparison only included

the dihedral angles across residues 15 - 98 (or 96) depending on data availability, as some of the groupings only had one structure that spanned a particular templating region and thus did not have a standard deviation value to be used for the analysis. It is hypothesized that the comparisons with a greater percentage of values less than 0.05 would likely be a more influential factor in contributing to strain formation. For each of the comparisons, it was generally observed that one of the categories appeared to be less variable than the other (patient structure, with mutations/PTMs, patient or potential for a small molecule, and the presence of a chain redirection at residue 65-70). Thus the reasoning behind this analysis was that comparisons with a statistically significant difference in standard deviation would indicate that the factor being compared did have an influence on the dihedral angle variability. A high percentage of residues that were influenced by this would "rank" that factor higher than the others, accounting for both phi and psi angles.

Across all comparisons, there was a greater percentage of p values greater than 0.05 for both angles phi and psi. For both angles phi and psi, the category of mutation/PTM vs. none had the smallest percentage of significant differences between variance. The Recombinant vs. Patient, 65-70 Chain Reversal vs. Redirection, and Small Molecule categories however had more similar distributions, however the values were not consistently the same between phi and psi angles. In general, the psi angles for all four categories had a higher percentage of p-values less than 0.05, which is an interesting contrast to the previous analyses suggesting there was no significant difference between phi/psi angle variance among α-synuclein amyloid structures.When looking at the particular location of the significant differences in variance across the comparisons, the only residue that was consistently different across all four categories for both angles phi and psi was ALA76 (Supplemental Figure S1). The regions of significant

difference in standard deviation appear to vary, even between the phi and psi comparisons for a particular category.

Discussion/Conclusions

In this investigation, we initially sought out to see if data extracted from dihedral angle measurements could be used to analyze and characterize amyloid forming proteins in order to gain a better understanding of prion biology from a structural perspective. Initial observations of glycine distributions on a Ramachandran plot comparing amyloid α-synuclein structures to globular α-synuclein structures revealed a higher population of residues in the disallowed regions among the amyloid derived glycines. Considering the reduced steric implications the variable group hydrogen confers, it was also expected that the majority of chain redirections/reversals both had at least one glycine present (Table II), in order to provide added stability. With the location of glycines within chain redirections in particular, the majority of glycines appeared to be located at the apex/vertex point of a chain redirection, followed by somewhere before the vertex point then after (Figure 3A). When splitting the data to compare the distributions between recombinant and patient derived α-synuclein amyloids, the position of glycines was extremely skewed towards the vertex position among patient derived amyloids (Figures 3B, 3C). This raises the question with regards to the impact of fibril source on amyloid structure, with a clear difference in this aspect between the patient derived fibrils and those recombinantly generated. Intriguingly however, one element that was observed to be conserved across the majority of recombinant α-synuclein fibrils and all of the patient derived fibrils was the presence of a chain reversal at residues 65-70.

As the observation of conserved chain reversal motifs in particular regions of the α-synuclein protein sequence was observed, this raised the question regarding the extent to which the dihedral angles themselves were conserved, and if this variance could be compared across various classifications of amyloids. One of the largest questions in the prion field revolves around the initial misfolding process (Figure 1D) and the specific intrinsic and extrinsic factors that drive this process as the exact mechanism of misfolding remains unclear. Theoretically, elements within an amyloid fibril that are highly conserved across various structures of a particular amyloid protein are likely critical to fibril stability, and could potentially be a priority in terms of what is formed first during misfolding. Focusing dihedral angle measurements when approaching this question, the influence of four extrinsic/intrinsic factors on phi/psi variability was analyzing differences in standard deviation across various comparisons among α-synuclein amyloids. Among the four factors, the comparison between structures with a mutation/PTM compared to those without either had the lowest differences in standard deviation for both angles phi and psi. Focusing on the phi angle comparisons, both the 65-70 chain redirection/reversal and small molecule comparisons had the same percentage of significant differences in variation, but were outweighed by the recombinant vs. patient comparison. These trends differed slightly however looking at the psi angle comparisons, with the 65-70 chain redirections vs. reversals having the highest percentage of significant differences (Table III). Based on these findings, while out of these four comparisons the presence of mutations/PTMs appear to be the least influential factor on dihedral angle variance, it is difficult to make a conclusive statement with regards to the ranking of the other three based on differences between the phi and psi percent variances. Drawing from the differences in the glycine positioning analysis (Figure 3), fibril source could likely be a top contributing factor to strain formation, however this comparison was

not performed for the other two variables as well and would need to be in order to make a more conclusive statement.

Looking closer at the residue 26-35 region, this appeared to have a pretty big difference in significant variance between the recombinant vs. patient and mutation/PTM vs. none comparisons (Supplementary Figure S1). For both the phi and psi angles in the recombinant vs. patient comparison, the majority of residues in this range were significantly different between the two categories, whereas for the mutations/PTM vs. none comparison, the majority of residues in this range did not significantly differ from each other. These residues are absent from the other two comparisons due to the distribution of the data including structures that did not span those residues for the templating region. Notably however, the only amyloids that actually span that templating region are the 3 MSA structures (6XYP, 6XYO, 6XYQ), the Tuttle *et al.* 2016 ssNMR structure (2N0A), and the dimer/trimer structures of the T39 phosphorylated amyloids. In all of these structures that contain these residues, there appears to be a chain redirection or reversal present at that location as well, which is towards the edge of the protofilament interface region. Considering that this region is absent from the majority of the structures, this could also conceptually reduce an element of constraint amongst those structures, from the perspective of requiring fewer residues to have to accommodate in a tightly packed fibril structure.

While the regions of variance seem to generally be in similar locations across the comparisons, one residue that is consistently significantly variable across all of the columns (Supplementary Figure S1) is residue ALA76 which varies with regards to its positioning within each amyloid. Generally however, it does appear to be frequently located right next to or at the edge of a chain redirection or reversal motif. This finding perhaps raises the question regarding

the extent to which this residue could be altered in order for it to contribute to overall fibril instability, considering it is consistently variable across all of the comparisons.

There are several limitations that should be recognized when interpreting the findings. One of these includes the availability of the structures. These analyses were made using the structures currently available on PDB, which most likely do not encapsulate all of the structures and strains of α-synuclein in existence, limiting the applicability of the findings. And while this analysis was performed on α-synuclein amyloids, it is plausible that other amyloid forming proteins could potentially obey a different set of rules or be influenced by other factors to varying degrees remaining to be tested. Additionally, the four factors chosen to be compared in this study are by no means all of the factors that could potentially play a role in initial strain formation. In order to ultimately gain a stronger understanding of the initial misfolding mechanism of α-synuclein prions, additional factors such as solvent conditions, the presence of other structural elements such as particular interface regions or intramolecular interactions, along with pairing combinations of these factors (for example structures containing an E46-K80 salt bridge, and a chain reversal at residues 65-70) in order to fine tune and parse apart the hierarchical organization of these factors. As described above, while the findings direct to the presence of mutations/PTMs as the lowest contributing factor, and the other three categories of being indifferentiable, including multiple factors at once for comparisons could perhaps shed light on this aspect.

Here we have employed a Ramachandran-based analysis to characterize structural elements of amyloid proteins (specifically α-synuclein). Visual observations of chain reversal motifs in particular have highlighted one contributor to structural diversity among amyloid structures. However these observations were based on qualitative analyses. Ongoing

collaborations with CCP are aimed at quantifying these observations in order to establish a new set of rules and definitions specific to amyloid proteins. These could improve upon the preliminary classifications defined in this investigation to a more objective definition based purely on the dihedral angle data. Future investigation building off of this work should aim to expand this analysis to include other factors including those mentioned above, as well as extending this to other amyloid forming proteins such as tau, amyloid ß, etc., in order to test if these factors contribute to the similar degrees as one another across different amyloid forming proteins, or if these elements are specific to proteins. Utilizing this approach, a better understanding of the contributors to prion misfolding can be gained, in hopes of ultimately elucidating the mechanism of prion propagation and what drives strain formation.

In addition to the aforementioned potential future directions, additional analyses that can be incorporated into this investigation could be looking at the conservation of hydrophobicity in particular structural motifs. Comparisons of particular conserved structural regions in amyloids to amino acid chemistry could perhaps reveal relationships between if protein chemistry is a requisite or major contributor to the formation of particular structures observed in amyloids. Coupling this with the Ramachandran approach, the identification of potential hydrophobic regions for example can be analyzed for their degree of conservation of dihedral angles, especially as the core region of many amyloid structures appear to be more hydrophobic in nature (Tuttle et al., 2016; Guerrero-Ferreira et al., 2018). As the actual process of protein misfolding has yet to be captured, static structures such as the ones published in the PDB will remain key to understanding this mechanism, through the lens of conserved and variable domains across prion strains.

FIGURES AND TABLES

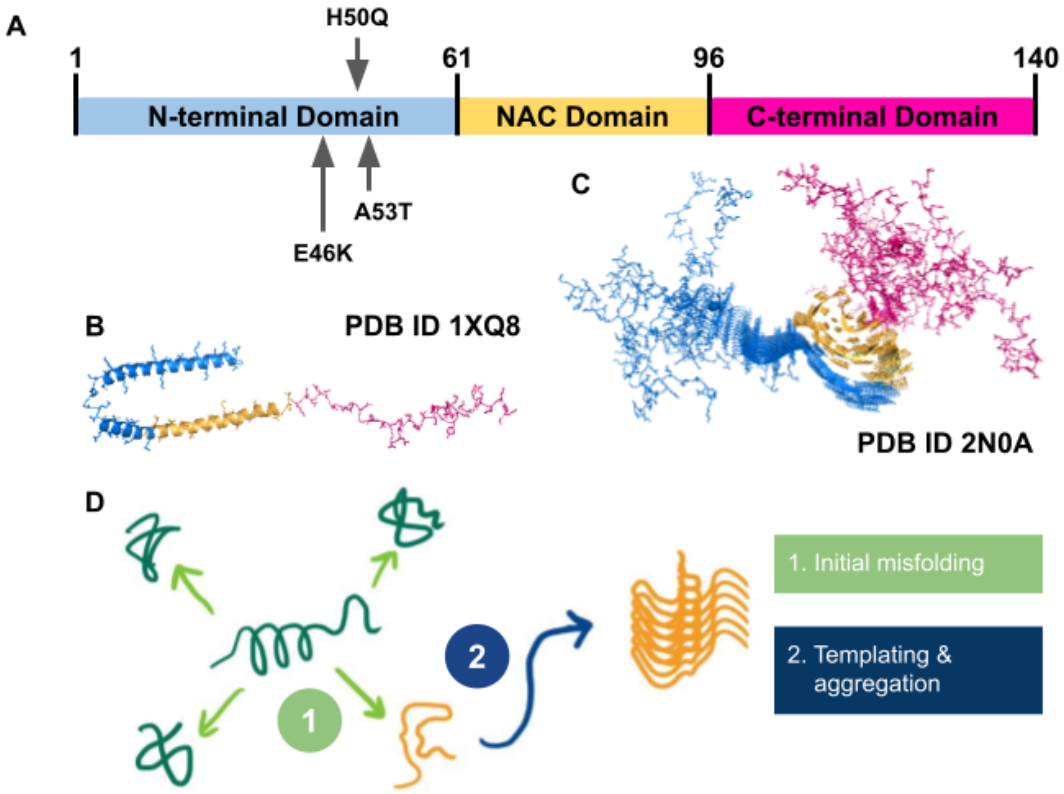

Figure 1. An Overview of Protein Misfolding Among α-synuclein Amyloids
(A) The three general domains of the 140-amino acid long polypeptide sequence for α-synuclein is shown, with mutations discussed in this paper highlighted in the N-terminal domain. In general, the NAC Domain makes up the majority of the hydrophobic core characteristic of amyloid structures. (B) The structure of human micelle bound α-synuclein is shown using PyMol software, with the 3-domains color coded. (C) The structure of a full length human α-synuclein fibril solved via ssNMR is shown using PyMol software. (D) The general process of protein misfolding consists of the initial misfolding step whereby the native soluble state protein adopts a misfolded ß-sheet rich conformation, followed by rounds of templating that gives rise to aggregates of these fibrils.

Table I. Dihedral Angle Classifications for ß- and - turns

Turn type	, (i + 1)	, (i + 2)
ß-Turns[b]		
I	-60º, -30º	-90º, 0º
II	-60º, 120º	80º, 0º
VIII	-60º, -30º	-120º, 120º
I'	60º, 30º	90º, 0º
II'	60º, -120º	-80º, 0º
VIa1[a]	-60º, 120º	-90º, 0º
VIa2[a]	-120º, 120º	-60º, 0º
VIba	-135º, 135º	-75º, 160º
IV	Turns excluded from categories above	
-Turns[c]		
Classic	75º, -64º	---
Inverse	-79º, 69º	---

* *adapted from Hutchinson & Thornton 1996*

a. Values defined by Richardson 1981
b. Values defined by Venkatachalam 1968, besides noted
c. Values defined by Némethy and Printz 1972

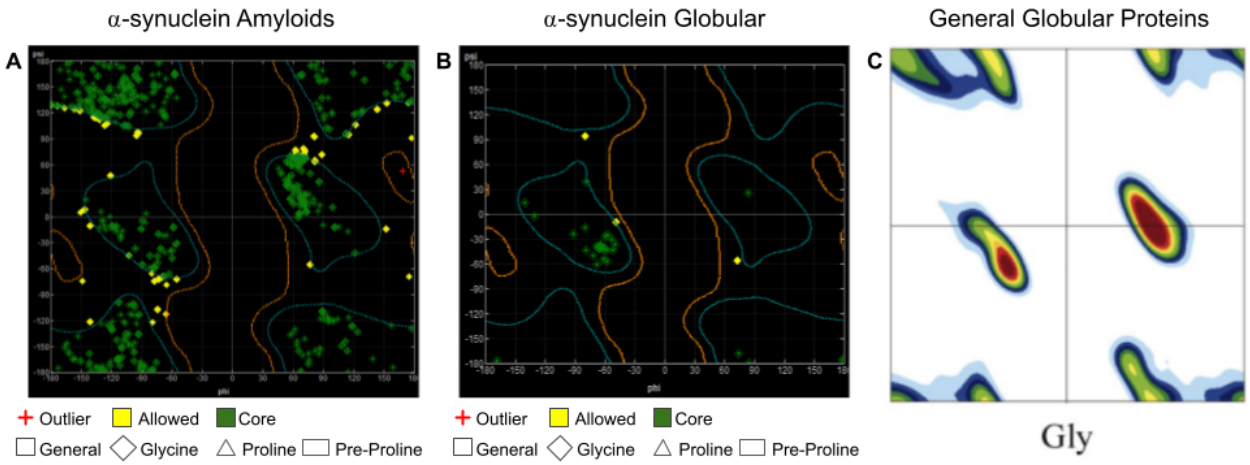

Figure 2. Glycines Occupy a Larger Region on the α-synuclein Amyloid Ramachandran Plot Using MOE software, Ramachandran plots of glycine residues from amyloids and globular structures for α-synuclein published on the PDB were generated. (A) Ramachandran plot generated from all α-synuclein amyloids, omitting short chain residues. (B) All glycines from α-synuclein globular structures were plotted. (C) A Ramachandran plot from globular proteins, adapted from Hovmöller et al. 2002.

Table II. The majority of Chain Redirections and Reversals Among α-synuclein Amyloids Do Contain at Least One Glycine

	Percentage with Glycines	Percentage without Glycines
Chain Reversal	83.6%	16.4%
Chain Redirection	78.9%	21.1%

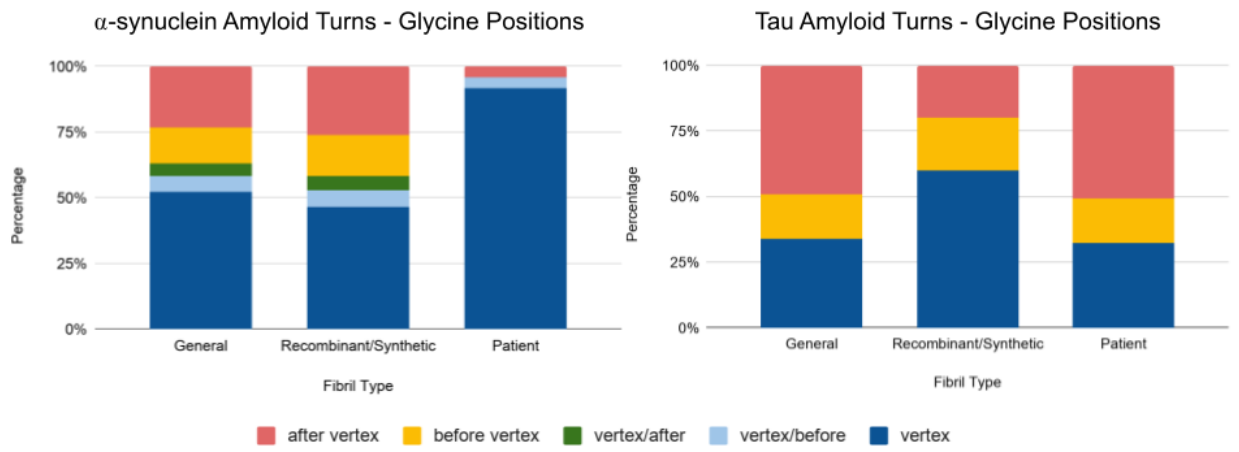

Figure 3. Glycines Tend To Be Located At the Vertex Among α-synuclein Amyloids
The location of glycine residues within chain redirections of tau and α-synuclein amyloid structures were noted and calculated as a percentage of all chain redirection with glycine residues. (A) Right and Left (R/L) chain redirection among all α-synuclein amyloids, (B) R/L chain redirection among recombinant α-synuclein amyloids, (C) R/L chain redirection among patient derived α-synuclein amyloids, (D) R/L chain redirection among all tau amyloids, (E) R/L chain redirection among all recombinant tau amyloids, (F) R/L chain redirection among patient derived tau amyloids.

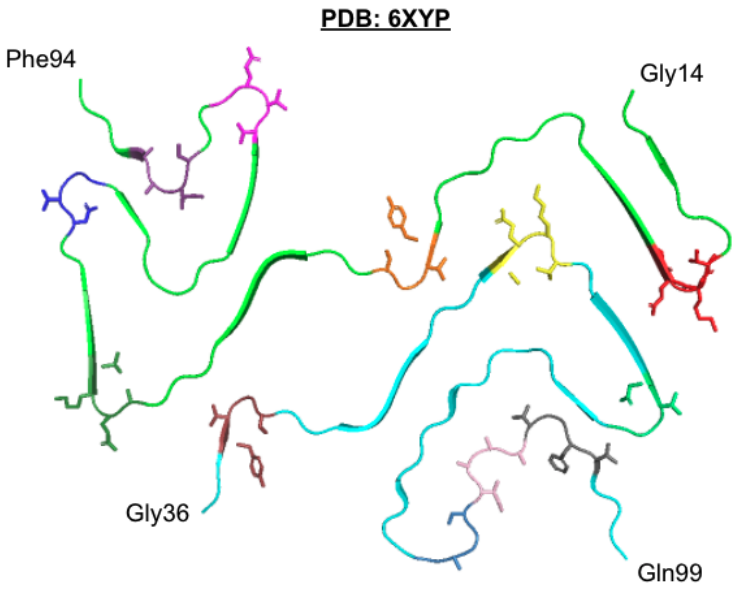

Table of beta turns - Chain A (green)

No.	Turn	Sequence	Turn type
1	Thr22-Gly25	TKQG	VIII
2	Tyr39-Ser42	YVGS	IV
3	Ala56-Thr59	AEKT	VIII
4	Asn65-Gly68	NVGG	IV
5	Thr81-Gly84	TVEG	IV
6	Ser87-Ala90	SIAA	IV

Table of beta turns - Chain B (teal)

No.	Turn	Sequence	Turn type
1	Tyr39-Ser42	YVGS	IV
2	Ala56-Thr59	AEKT	IV
3	Asn65-Gly68	NVGG	IV
4	Gly84-Ser87	GAGS	II
5	Ile88-Ala91	IAAA	IV
6	Ala91-Phe94	ATGF	IV

Figure 4. Current Turn/Loop Predictor and Definitions Do Not Capture all Amyloid Chain Redirections/Reversals

The MSA II Type I filament (PDB ID 6XYP) was loaded onto the PROMOTIF software (housed on the JPred4 online server) in order to determine if the chain redirections and reversals motifs could be detected. One chain from each of the asymmetrical filaments are shown with the corresponding chain redirections color coded on the table of beta turns (Chain A = green, Chain B = light blue).

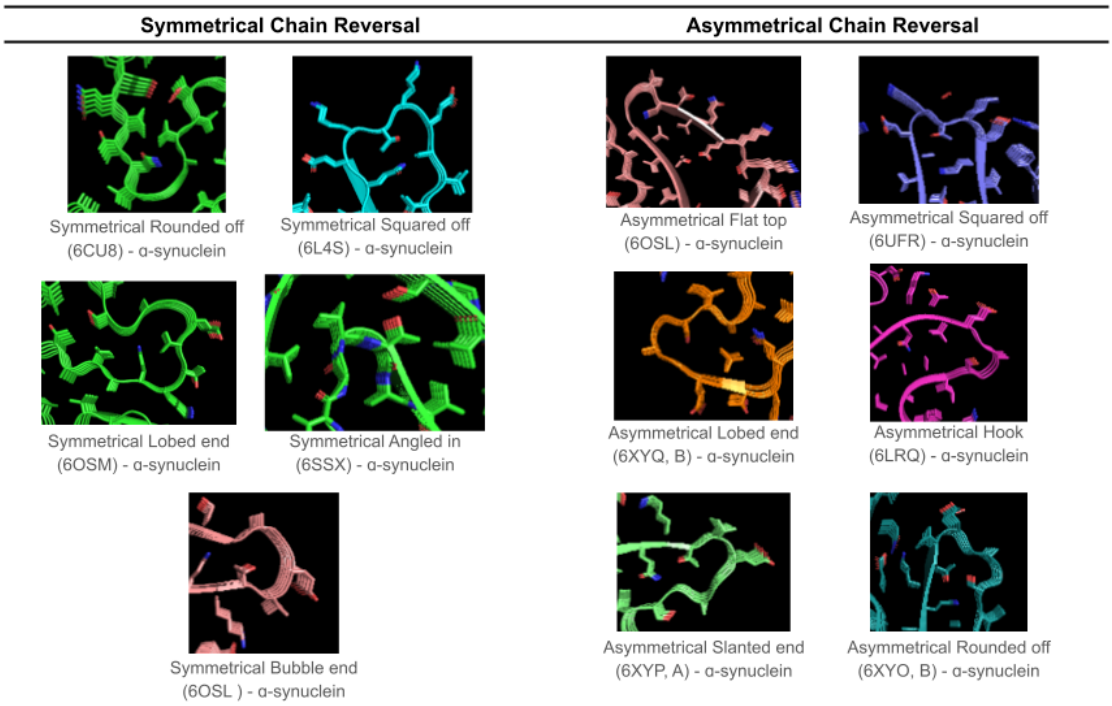

Figure 5. Classification of Chain Reversal Types Observed Among α-synuclein Amyloids
The classifications for chain reversals observed among α-synuclein amyloids are shown, with example images (PDB ID noted). Structures were obtained by loaded PDB ID onto PyMol software, and then analyzed by going through the polypeptide chain of each α-synuclein amyloid.

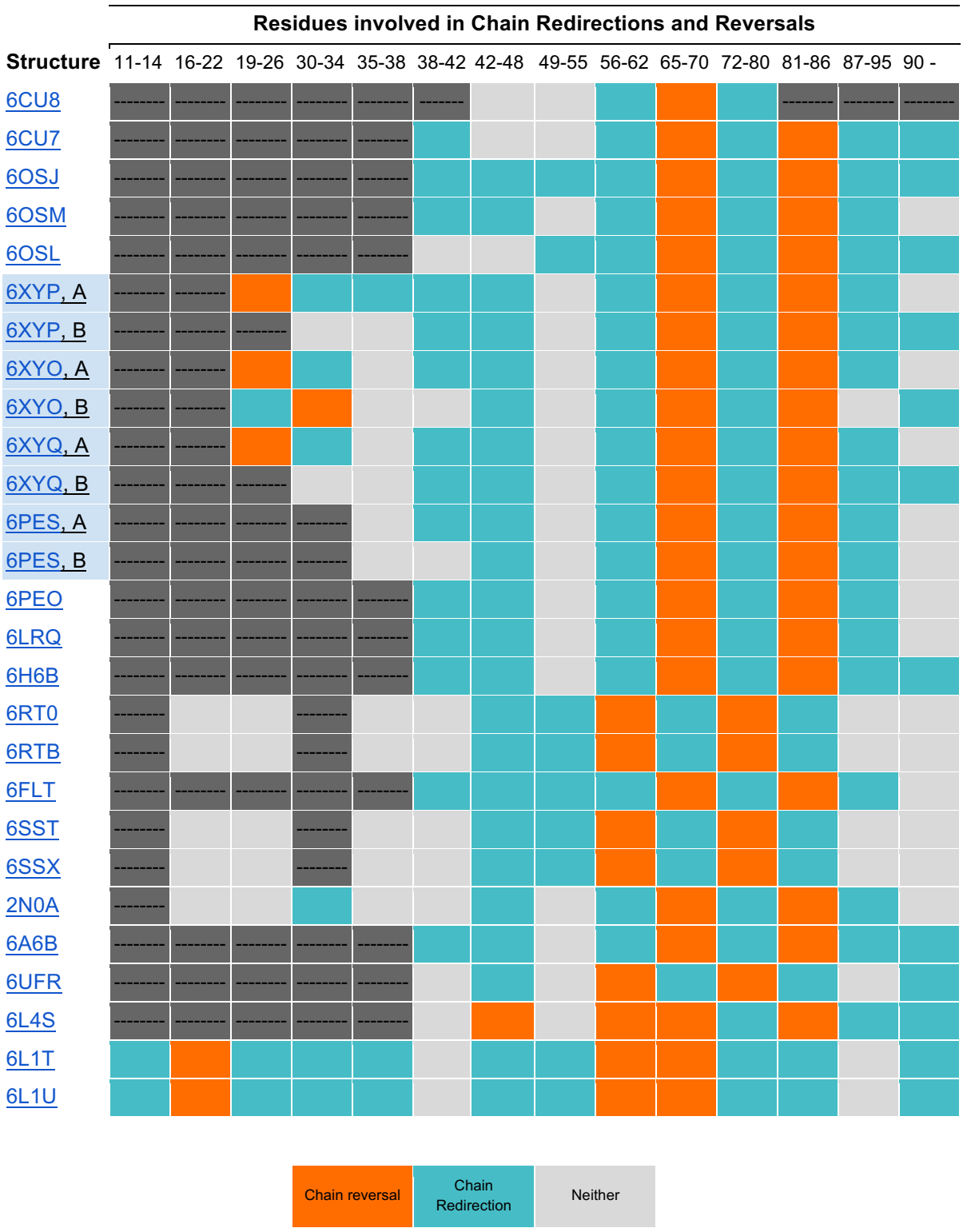
Residues involved in Chain Redirections and Reversals
Structure
11-14
16-22
19-26
30-34
35-38
38-42
42-48
49-55
56-62
65-70
72-80
81-86
87-95
90 -
6CU8
6CU7
6OSJ
6OSM
6OSL
6XYP, A
6XYP, B
6XYO, A
6XYO, B
6XYQ, A
6XYQ, B
6PES, A
6PES, B
6PEO
6LRQ
6H6B
6RT0
6RTB
6FLT
6SST
6SSX
2N0A
6A6B
6UFR
6L4S
6L1T
6L1U
Chain reversal
Chain Redirection
Neither

Figure 6. Location of Chain Redirections and Reversals Among α-synuclein Amyloids
The residues involved in chain redirections and reversals motifs within each of the α-synuclein amyloid structures mined from the PDB were determined and organized on a table. Asymmetrical filaments are separated into different rows, designated as the PDB ID followed by A or B to denote the separate filaments. Dark grey boxes with dashed lines indicate the absence of those residues in the templating region of the amyloid, while light grey boxes with "no" indicate the presence of that region in the structure however not being involved in a chain redirections or reversals motif. Teal boxes indicate the presence of a chain reversal while orange boxes denote the presence of a chain redirection. Note, the exact placement of a chain redirection/reversal varies across the structures by a couple residues (and does not strictly adhere to the ranges designated at the top of the columns).

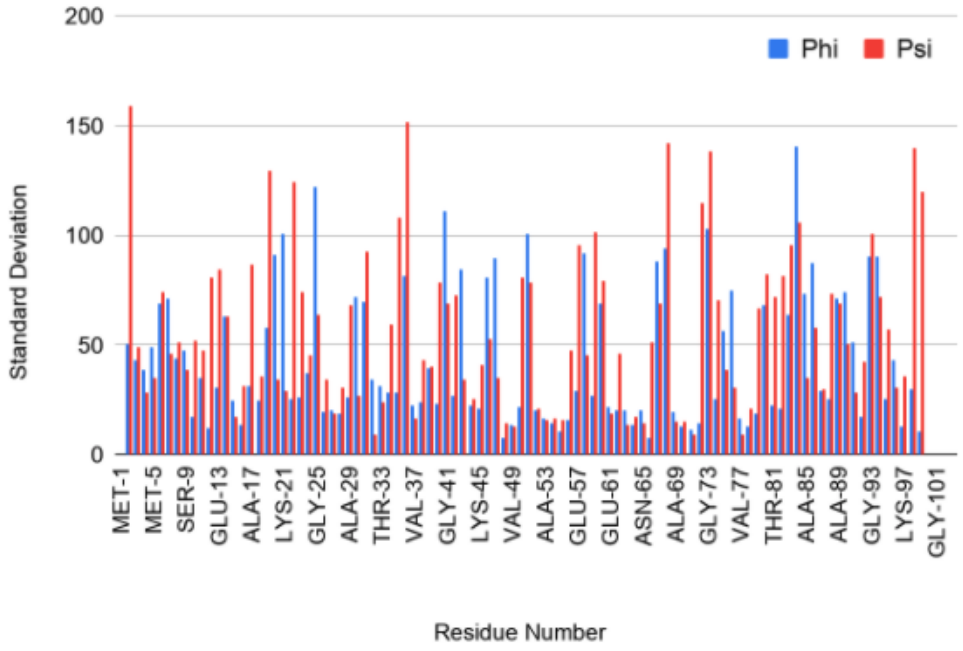

Figure 7. Standard Deviation of Dihedral Angles Across All α-synuclein Amyloids
The standard deviation of the dihedral angles phi and psi were plotted against the corresponding residues for α-synuclein amyloids in order to analyze for potential differences in variation. The plot shown here includes all α-synuclein amyloids, with standard deviation across phi angles shown in blue and psi angles in red. Only the residues with data are shown.

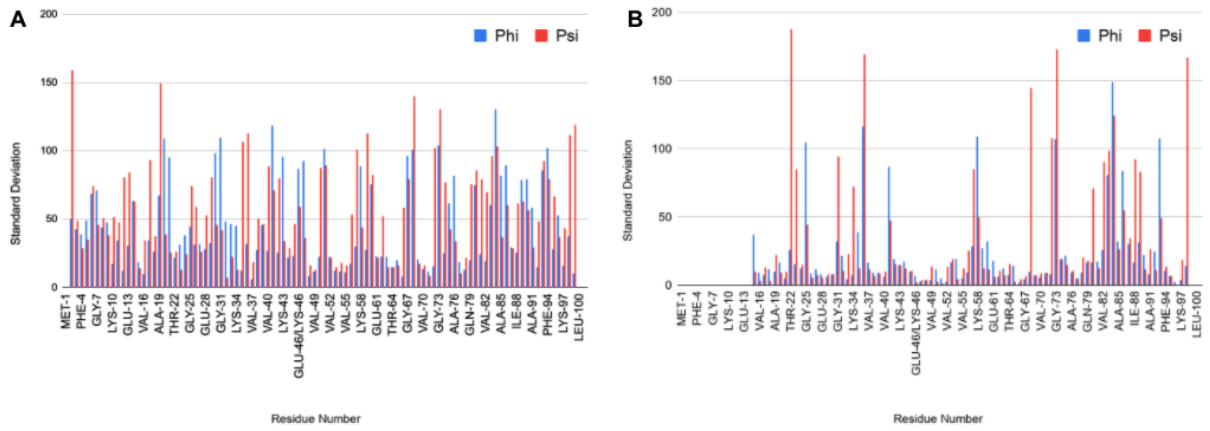

Figure 8. Standard Deviation Comparison Between Patient Derived and Recombinant α-synuclein Amyloids

The standard deviations of the grouped amyloids, (A) recombinant and (B) patient derived, were plotted against the corresponding residue, with the phi angles shown in blue and psi angles shown in red.

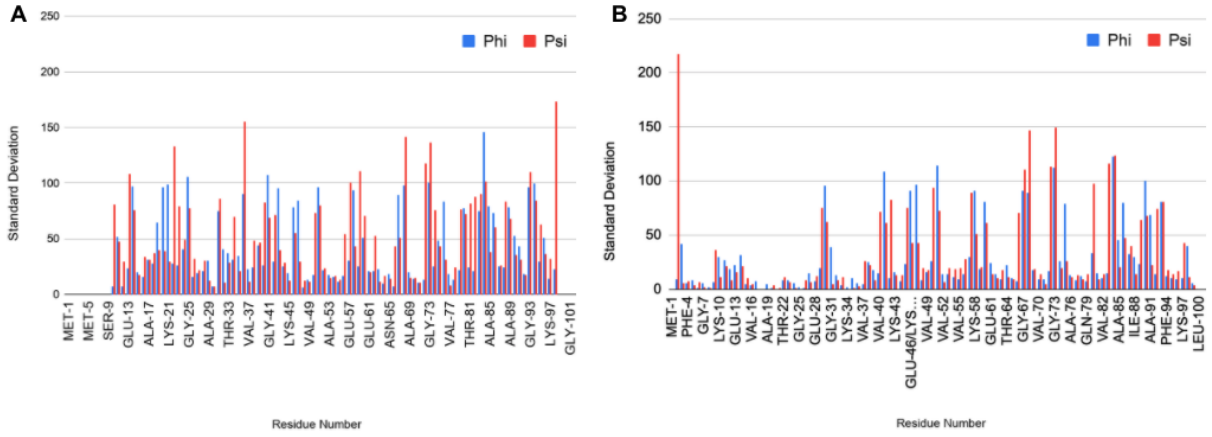

Figure 9. Standard Deviation Comparison Between α-synuclein Amyloids With and Without Mutations/Post-Translational Modifications

The standard deviations of the grouped amyloids, (A) structures with either a mutation or post-translational modifications (PTMs) and (B) structures without either, were plotted against the corresponding residue, with the phi angles shown in blue and psi angles shown in red. Mutations include A53T, E46K, and H50Q, while PTMs include a T39 phosphorylated dimer and trimer.

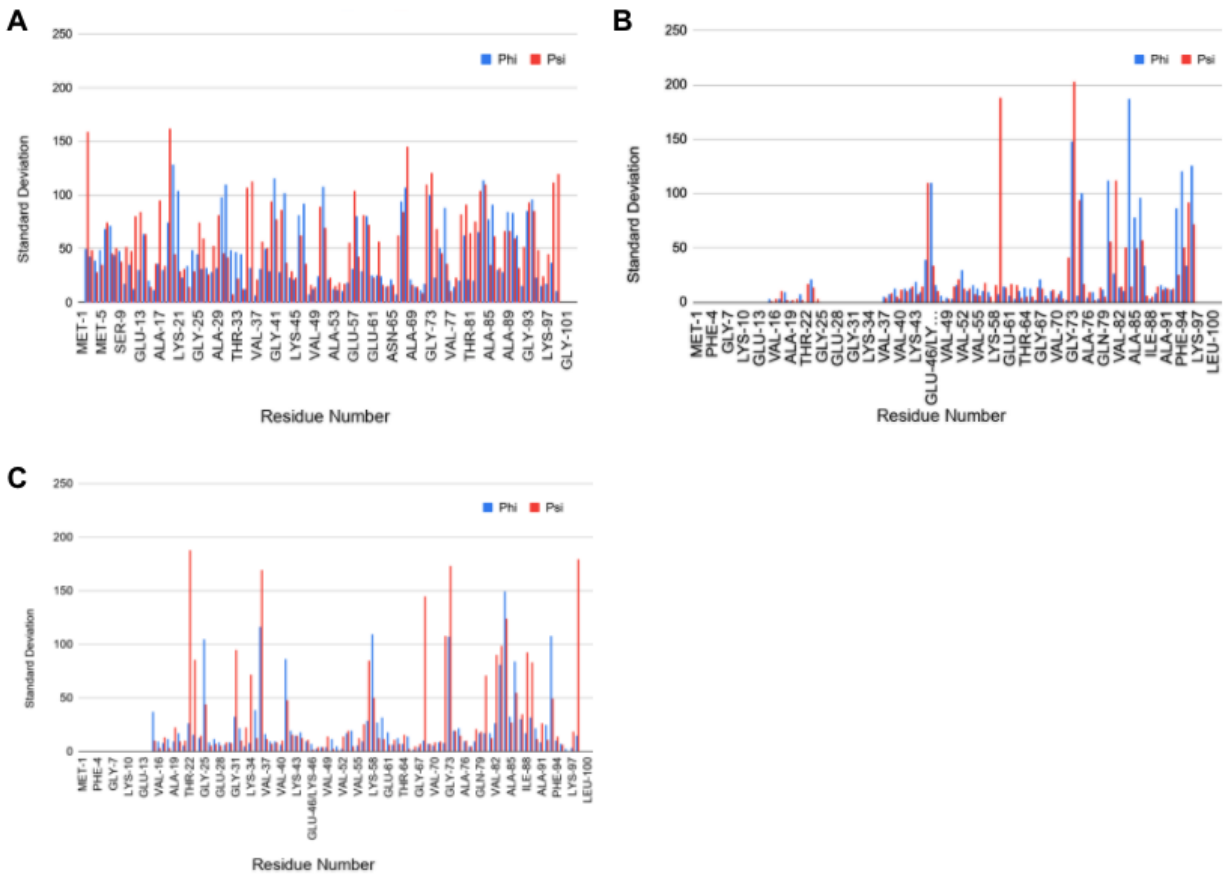

Figure 10. Standard Deviation Comparison Between α-synuclein Amyloids With or Without a Small Molecule (Cofactor)

The standard deviations of the grouped amyloids, (A) structures with no small molecule present at the protofilament interface, (B) structures with the potential for a small molecule at the protofilament interface, and (C) patient derived structures with a small molecule present at the protofilament interface, were plotted against the corresponding residue, with the phi angles shown in blue and psi angles shown in red.

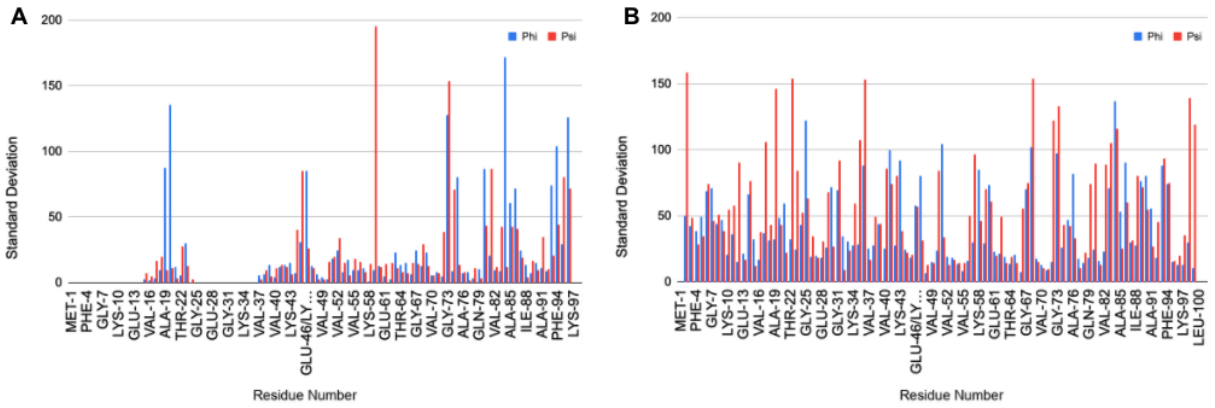

Figure 11. Standard Deviation Comparison Between α-synuclein Amyloids With a Chain Redirection or Reversal at the 65-70 Residue Domain

The standard deviations of the grouped amyloids, (A) structures with a chain redirection at residues 65-70 and (B) structures a chain reversal at residues 65-70, were plotted against the corresponding residue, with the phi angles shown in blue and psi angles shown in red.

Table III. Significance in Dihedral Angle Variability Among α-synuclein Amyloids Across Extrinsic and Intrinsic Factors

		Recombinant vs. Patient	Mut/PTM vs. None	65-70 Chain Redirection vs. Reversal	Small Molecule?
PHI	$p \geq 0.05$	65.48%	79.76%	67.14%	67.14%
	$p < 0.05$	34.52%	20.24%	32.86%	32.86%
PSI	$p \geq 0.05$	61.90%	72.62%	55.71%	60%
	$p < 0.05$	38.10%	27.38%	44.29%	40%

Mut = mutation

SUPPLEMENTARY FIGURES/TABLES

Supplementary Table I. Protein Data Bank Codes for all α-synuclein Amyloids

4 letter code	Description	Protein Type	Methods	Resolution	Publication
6CU8	Alpha Synuclein fibril formed by full length protein	Twister Polymorph	Electron microscopy	3.60 Å	Li *et al.* 2018a
6CU7	Alpha Synuclein fibril formed by full length protein	Rod Polymorph	Electron microscopy	3.50 Å	Li *et al.* 2018a
6OSJ	Cryo-EM structure of the N-terminally acetylated full length alpha-synuclein fibrils	Ac1-140	Electron microscopy	2.80 Å	Ni *et al.* 2019
6OSM	Cryo-EM structure of the N-terminally acetylated C-terminal Alpha-synuclein truncation	Ac1-103	Electron microscopy	3.40 Å	Ni *et al.* 2019
6OSL	Cryo-EM structure of the N-terminally acetylated C-terminal Alpha-synuclein truncation	Ac1-122	Electron microscopy	3.00 Å	Ni *et al.* 2019
6XYP	Multiple system atrophy Type II-1 alpha-synuclein filament	Type II-1	Electron microscopy	3.29 Å	Schweighauser *et al.* 2020
6XYO	Multiple system atrophy Type I alpha-synuclein filament	Type I	Electron microscopy	2.60 Å	Schweighauser *et al.* 2020
6XYQ	Multiple system atrophy Type II-2 alpha synuclein filament	Type II-2	Electron microscopy	3.09 Å	Schweighauser *et al.* 2020
6PES	Cryo-EM structure of alpha-synuclein H50Q Wide Fibril	H50Q Wide Fibril	Electron microscopy	3.60 Å	Boyer *et al.* 2019
6PEO	Cryo-EM structure of alpha-synuclein H50Q Narrow Fibril	H50Q Narrow Fibril	Electron microscopy	3.30 Å	Boyer *et al.* 2019
6LRQ	Cryo-EM structure of A53T alpha-synuclein amyloid fibril	A53T amyloid Fibril	Electron microscopy	3.49 Å	Sun *et al.* 2020
6H6B	Structure of alpha-synuclein fibrils	alpha-synuclein fibril	Electron microscopy	3.40 Å	Guerrero-Ferreira *et al.* 2018

6RT0	Cryo-EM structure of alpha-synuclein fibril polymorph 2A	polymorph 2A	Electron microscopy	3.10 Å	Guerrero-Ferreira *et al.* 2019
6RTB	Cryo-EM structure of alpha-synuclein fibril polymorph 2B	polymorph 2B	Electron microscopy	3.46 Å	Guerrero-Ferreira *et al.* 2019
6FLT	Structure of alpha-synuclein fibrils	alpha-synuclein fibril	Electron microscopy	3.42 Å	Guerrero-Ferreira *et al.* 2018
6SST	Cryo-EM structure of alpha-synuclein fibril polymorph 2B	polymorph 2B	Electron microscopy	3.40 Å	Guerrero-Ferreira *et al.* 2019
6SSX	Cryo-EM structure of alpha-synuclein fibril polymorph 2A	polymorph 2A	Electron microscopy	2.98 Å	Guerrero-Ferreira *et al.* 2019
2N0A	Atomic-resolution structure of alpha-synuclein fibrils	alpha-synuclein fibrils	Solid State NMR	-----	Tuttle *et al*. 2016
6A6B	Cryo-EM structure of alpha-synuclein fiber	alpha-synuclein fiber	Electron microscopy	3.07 Å	Li *et al*. 2018b
6UFR	Structure of recombinantly assembled E46K alpha-synuclein fibrils	E46K alpha-synuclein fibrils	Electron microscopy	2.50 Å	Boyer *et al*. 2020
6L4S	Cryo-EM structure of alpha-synuclein fiber mutation type E46K	E46K alpha-synuclein fibrils	Electron microscopy	3.37 Å	Zhao *et al*. 2020a
6L1T	Cryo-EM structure of phosphorylated Tyr39 a-synuclein amyloid fibril - twister dimer of pY39 α-syn fibrils	Residues 1-100 (largest identified core region)	Electron microscopy	3.22 Å	Zhao *et al*. 2020b
6L1U	Cryo-EM structure of phosphorylated Tyr39 alpha-synuclein amyloid fibril - twist-trimer of pY39 α-syn fibrils	Residues 1-100 (largest identified core region)	Electron microscopy	3.37 Å	Zhao *et al*. 2020b

*blue shaded PDB ID boxes indicate patient derived fibrils, while white boxes indicate recombinant

Supplementary Table II. Protein Data Bank Codes for all α-synuclein Globular Proteins

4 letter code	Description	Protein Type	Methods	Resolution	Publication
1XQ8	Human micelle-bound alpha-synuclein	Micelle-bound a-syn	Solution NMR	-----	Ulmer *et al.* 2005
2KKW	SLAS-micelle bound alpha-synuclein	Micelle-bound a-syn	Solution NMR	-----	Rao *et al.* 2010

	Recombinant vs. Patient		MUT/PTM vs. None		65-69 LOOP vs. TURN		Small Molecule?	
Residue	p (PHI)	p (PSI)	p (PHI)	p (PSI)	p (PHI)	p (PSI)	p (PHI)	p (PSI)
VAL15	0.27955623	0.487738759	0.475676959	0.302286565	0.006259764	0.122037115	0.157399403	0.213097104
VAL16	0.86473081	0.090627011	0.215850201	0.387121004	0.132072215	0.05483006	0.316749574	0.188261886
ALA17	0.034116128	0.046450411	0.450146674	0.190419703	0.009685166	0.016264557	0.08244692	0.005454162
ALA18	0.537771403	0.054545958	0.253663048	0.157328123	0.355984652	0.085141735	0.431019597	0.329641661
ALA19	0.091745758	0.041010837	0.161282698	0.186454679	0.06672195	0.005917421	0.000248877	0.003057996
GLU20	0.125562264	0.329997305	0.201561409	0.376308099	0.062038988	0.232425769	0.062651487	0.240855787
LYS21	0.025027641	0.072952257	0.005334569	0.006001137	0.167194912	0.164227234	0.002742091	0.001671799
THR22	0.026230446	4.57E-08	0.557112461	0.129996254	0.203608915	0.013987985	0.298251443	2.86E-07
LYS23	0.149965911	0.009397498	0.196104113	0.015049116	0.846246738	4.85E-05	0.022750475	0.042287226
GLN24	0.001951518	0.598944211	0.211670131	0.038556443	0.194617922	0.016600205	0.103460851	0.147967249
GLY25	0.239713121	0.232597758	0.00591743	0.05825277				
VAL26	2.07E-05	0.009508163	0.163976208	0.305183746				
ALA27	2.50E-05	0.037532138	0.603977273	0.378171933				
GLU-28	1.55E-05	0.012542628	0.411666914	0.385952646				
ALA29	1.15E-05	0.032538645	0.60204855	0.000108053				
ALA30	8.04E-06	0.030721603	1.01E-05	0.000106895				
GLY31	0.000826955	0.281249543	0.578484311	0.055049568				
LYS-32	9.04E-06	0.77862072	0.283951069	0.503296482				
THR33	1.39E-06	0.00017854	0.22107799	0.481894584				
LYS34	1.39E-06	0.095750969	0.219611797	0.196458482				
GLU35	0.003883163	0.008842202	0.142629921	0.084054275				
GLY36	0.956906534	0.444498609	0.275521036	0.024885768				
VAL37	0.053656784	0.178423061	0.000309699	0.002006002	0.000177353	0.026486967	0.068136282	0.029051515
LEU38	0.05102348	0.158662657	0.665840056	0.395854043	0.109253356	0.274796813	0.074833897	0.153728339
TYR39	0.108215061	0.084948231	0.403667097	0.077608019	0.429711284	0.104700212	0.27233342	0.052750345
VAL40	0.114211741	0.003356354	0.525905814	0.570810344	0.114082714	0.012603799	0.060622307	0.000440533
GLY41	0.111869145	0.332599416	0.145084808	0.947628502	0.044553957	0.032387291	0.030544099	0.141132312
SER-42	0.415876036	0.009316582	0.023221177	0.92727646	0.169247763	0.015979928	0.608752931	0.001511889
LYS43	0.010684209	0.265104596	0.017586249	0.107723219	0.043297428	0.091382672	0.008152268	0.161369428
THR44	0.521030076	0.059056149	0.036375167	0.052586171	0.0957688	0.204806827	0.472269027	0.057943082
LYS45	0.158591519	0.259426385	0.545532005	1.40E-05	0.366130506	0.001239025	0.04758855	1.75E-05
GLU/LYS46	0.000225383	0.010408545	0.562878511	0.78235193	0.306117418	0.300273244	0.006511069	0.022144271
GLY47	6.07E-14	3.90E-05	0.411593986	0.034363276	0.008060801	0.121109061	5.30E-10	2.46E-04
VAL48	0.119660486	0.014708459	0.425295659	0.268427788	0.996421957	0.051822729	0.293028359	0.0137064
VAL49	0.080588073	0.997460747	0.969928203	0.273796149	0.010590136	0.038512271	0.030315307	0.295049101
HIS/GLN50	0.373428584	9.50E-06	0.230297055	0.266885268	0.026228477	0.000296113	0.086629288	6.48E-06
GLY51	4.51E-05	0.000436058	0.30555569	0.46882104	3.46E-06	0.231102276	9.02E-09	3.59E-02
VAL52	0.046103582	0.75588401	0.243505755	0.05640251	0.302872038	0.040015568	0.097139161	0.919724229
ALA53	0.27268273	0.49383102	0.174998998	0.603341302	0.064246429	0.862326228	0.476358178	0.726687504
THR54	0.502217718	0.017010919	0.141961395	0.78886362	0.290938625	0.182582831	0.496374776	0.056950304
VAL55	0.078190944	0.772760419	0.442106615	0.142777062	0.914041017	0.656619099	0.190394672	0.502763186
ALA56	0.315162918	0.391941515	0.780336456	0.531011263	0.361619688	0.535781586	0.196929133	0.697620997
GLU57	0.585142829	0.670001523	0.936478735	0.26293373	0.02067061	0.000113212	0.088134338	0.001788613
LYS58	0.132337505	0.386364432	0.168189593	0.792692236	0.001302888	0.016356927	0.002126048	0.048075043
THR59	0.772641488	0.001312927	0.215637755	0.001140523	0.014377432	4.15E-05	0.067485887	0.000495608
LYS60	0.100265382	0.000316196	0.012828334	0.993128853	0.073679917	0.037770789	0.033626357	0.009453506
GLU61	0.359107189	0.038527227	0.729797328	0.440414133	0.007484503	0.598900501	0.028084086	0.104595048
GLN62	0.191868802	0.204001254	0.642492699	0.182337258	0.112193929	0.487204076	0.06833018	0.302133328
VAL63	0.488761668	0	0.245346868	0.032066148	0.635021066	0.531190102	0.543359574	0.063452474
THR64	0.066737273	0.927258535	1.91E-05	0.2496953	0.418080479	0.031699339	0.128059845	0.215778169
ASN65	0.35916111	0.004742778	0.067839618	0.38136765	0.277815002	0.192433044	0.413722577	0.008030178
VAL66	0.001403397	0.021112345	0.54063127	0.031061998	0.252965724	0.122917128	0.000794075	0.010862005
GLY67	3.34E-06	0.01314641	0.807575587	0.012540055	0.214009753	0.091726322	0.000238378	0.000238378
GLY68	0.00422994	0.502758445	0.476402585	0.928176767	0.014806509	0.000282627	0.000547253	0.026734251
ALA69	0.139087132	0.062419277	0.643499044	0.498625601	0.577155545	0.532514695	0.321633618	0.274352755
VAL70	0.064899709	0.184323645	0.311502788	0.900766109	0.097310629	0.256631269	0.012190836	0.439952472
VAL71	0.432347088	0.663697519	0.569885711	0.083175445	0.615142316	0.627036111	0.786964385	0.495553277
THR72	0.233719008	0.460677913	0.871904603	0.696003378	0.106756966	0.039930536	0.088761899	0.171540932
GLY73	0.987152746	0.195057527	0.91599933	0.812372619	0.798809632	0.62695851	0.459925205	0.139763687
VAL74	0.275408075	0.013943893	0.950187541	0.005324203	0.017106909	0.168802078	0.200594135	0.102863147
THR75	0.342847932	0.279982843	0.254613342	0.80563125	0.133123534	0.375839614	0.075733282	0.418861813
ALA76	0.002269488	0.008992843	0.000703103	0.009165665	0.005375374	0.01588413	9.96E-05	0.001153476
VAL77	0.144623343	0.070913546	0.342567102	0.093026007	0.465938192	0.027119735	0.240558771	0.022766392
ALA78	0.2244761	0.578812418	0.825202765	0.01834669	0.020554644	0.169884693	0.075452469	0.47227496
GLN79	0.580363931	0.448502507	0.011013187	0.290941437	0.239597472	0.249934195	0.555644436	0.436557542
LYS80	0.023124396	0.143749723	0.088202884	0.067475933	0.002187109	0.005824538	0.02905641	0.077633629
THR81	0.375731547	0.016727459	0.070346683	0.004757504	0.677434466	0.000105818	0.746285001	0.057756572
VAL82	0.592876869	0.232359563	0.11859137	8.68E-09	0.057137791	9.76E-07	0.526798985	0.066218105
GLU83	0.443175182	0.820390328	0.049696554	0.232860371	0.088149083	0.22325881	0.416176115	0.606985177
GLY84	0.631092324	0.961550766	0.063997924	0.335192314	0.327359551	0.001593277	0.276965069	0.097326188
ALA85	0.063030005	0.22380631	0.198971662	0.030939779	0.777776838	0.28865224	0.263593131	0.427874028
GLY86	0.540855122	0.916467072	0.767269395	0.634102295	0.019991132	0.072676056	0.730952513	0.891210139
SER87	0.82320927	0.47199128	0.451542041	0.469931308	0.155540215	0.355433761	0.976434477	0.238011423
ILE88	0.51145358	0.030222167	0.404254034	0.000516928	0.118610715	0.002944532	0.1421569	0.03542472
ALA89	0.078708282	0.115229109	0.021321855	0.374627164	0.025881205	0.009574764	0.014074589	0.051775173
ALA90	0.034442896	0.052997244	0.002130523	0.158895463	0.042292182	0.079896543	0.011065117	0.050273313
ALA91	0.133516607	0.763620255	0.24986459	0.352680979	0.283078034	0.619405777	0.157422245	0.454450556
THR92	0.019144975	0.293153982	0.24506047	0.016376072	0.140871494	0.358446389	0.045788357	0.416550705
GLY93	0.074968231	0.109422165	0.165472388	0.186903511	0.191318433	0.00980888	0.137421221	0.019625728
PHE94	0.005524676	0.19372243	0.005716184	0.15225829	0.257320998	0.950411938	0.063575499	0.497019015
VAL95	0.013740296	0.022301216	0.008302007	0.024563634	0.009849071	0.00234425	0.085469904	0.034227982
LYS96	0.148333696	0.059399433	0.226341252	0.613651196	8.10E-11	2.00E-03	1.25E-05	1.49E-05
LYS97	0.108906813	0.031696232	0.743416607	0.323054068				
ASP98	0.001362277	0.058216342	0.014506212	2.12E-05				

Supplementary Figure S1. P-Values By Residue of Dihedral Angle Variability Analysis

This figure shows the calculated p-values after the F-test (Levene's Test) performed for each of the four comparisons listed at the top of the column. Separate F-tests were performed for phi and psi. Red boxes indicate statistically insignificant differences in standard deviation (greater than the critical value of $p = 0.05$) while green boxes indicate statistically significant differences in standard deviations between the comparisons. White boxes indicate regions of the sequence that did not contain dihedral angle data for the comparison/calculations.

REFERENCES

Basler, K., Oesch, B., Scott, M., Westaway, D., Wälchli, M., Groth, D.F., McKinley, M.P., Prusiner, S.B., and Weissmann, C. (1986). Scrapie and cellular PrP isoforms are encoded by the same chromosomal gene. Cell 46, 417–428.

Boyer, D.R., Li, B., Sun, C., Fan, W., Sawaya, M.R., Jiang, L., and Eisenberg, D.S. (2019). Structures of fibrils formed by α-synuclein hereditary disease mutant H50Q reveal new polymorphs. Nat Struct Mol Biol 26, 1044–1052.

Burré, J., Sharma, M., Tsetsenis, T., Buchman, V., Etherton, M., and Südhof, T.C. (2010). α-Synuclein Promotes SNARE-Complex Assembly in vivo and in vitro. Science 329, 1663–1667.

Burré, J., Sharma, M., and Südhof, T.C. (2015). Definition of a Molecular Pathway Mediating α-Synuclein Neurotoxicity. J. Neurosci. 35, 5221.

Collinge, J., and Clarke, A.R. (2007). A General Model of Prion Strains and Their Pathogenicity. Science 318, 930–936.

Dejerine, J., and Thomas, A. (1900). L'atrophie olivo-ponto-cérébelleuse. Nouvelle iconographie de la Salpêtrière 330–370.

Drozdetskiy, A., Cole, C., Procter, J., and Barton, G.J. (2015). JPred4: a protein secondary structure prediction server. Nucleic Acids Research 43, W389–W394.

Dugger, B.N., and Dickson, D.W. (2017). Pathology of Neurodegenerative Diseases. Cold Spring Harb Perspect Biol 9.

van der Eecken, H., Adams, R., and van Bogaert, L. (1960). Striopallidal-nigral degeneration. An hitherto undescribed lesion in paralysis agitans. J Neuropathol Exp Neurol. 159–161.

Eisenberg, D., and Jucker, M. (2012). The Amyloid State of Proteins in Human Diseases. Cell 148, 1188–1203.

Eliezer, D., Kutluay, E., Bussell, R., and Browne, G. (2001). Conformational properties of alpha-synuclein in its free and lipid-associated states. J Mol Biol 307, 1061–1073.

Forster, E., and Lewy, F. (1912). Paralysis agitans. Pathologische Anatomie Handbuch Der Neurologie. Berlin: Springer Verlag 920–933.

Getz, G., Starovolsky, A., and Domany, E. (2004). F2CS: FSSP to CATH and SCOP prediction server. Bioinformatics 20, 2150–2152.

Giasson, B.I., Duda, J.E., Quinn, S.M., Zhang, B., and Trojanowski, J.Q. Neuronal α-Synucleinopathy with Severe Movement Disorder in Mice Expressing A53T Human α-Synuclein. 13.

Gilman, S., Wenning, G.K., Low, P.A., Brooks, D.J., Mathias, C.J., Trojanowski, J.Q., Wood, N.W., Colosimo, C., Dürr, A., Fowler, C.J., et al. (2008). Second consensus statement on the diagnosis of multiple system atrophy. Neurology 71, 670–676.

Goedert, M. (2015). Alzheimer's and Parkinson's diseases: The prion concept in relation to assembled Aβ, tau, and α-synuclein. Science 349.

Graham, J.G., and Oppenheimer, D.R. (1969). Orthostatic hypotension and nicotine sensitivity in a case of multiple system atrophy. J Neurol Neurosurg Psychiatry 32, 28–34.

Guerrero-Ferreira, R., Taylor, N.M., Mona, D., Ringler, P., Lauer, M.E., Riek, R., Britschgi, M., and Stahlberg, H. (2018). Cryo-EM structure of alpha-synuclein fibrils. ELife 7, e36402.

Guerrero-Ferreira, R., Taylor, N.M., Arteni, A.-A., Kumari, P., Mona, D., Ringler, P., Britschgi,

M., Lauer, M.E., Makky, A., Verasdonck, J., et al. (2019). Two new polymorphic structures of human full-length alpha-synuclein fibrils solved by cryo-electron microscopy. ELife 8, e48907.

Holm, L., and Sander, C. (1997). Dali/FSSP classification of three-dimensional protein folds. Nucleic Acids Res 25, 231–234.

Hovmöller, S., Zhou, T., and Ohlson, T. (2002). Conformations of amino acids in proteins. Acta Crystallographica Section D 58, 768–776.

Hutchinson, E.G., and Thornton, J.M. (1996). PROMOTIF—A program to identify and analyze structural motifs in proteins. Protein Science 5, 212–220.

Kabsch, W., and Sander, C. (1983). Dictionary of protein secondary structure: Pattern recognition of hydrogen-bonded and geometrical features. Biopolymers 22, 2577–2637.

Kordower, J.H., Freeman, T.B., Snow, B.J., Vingerhoets, F.J.G., Mufson, E.J., Sanberg, P.R., Hauser, R.A., Smith, D.A., Nauert, G.M., Perl, D.P., et al. (1995). Neuropathological Evidence of Graft Survival and Striatal Reinnervation after the Transplantation of Fetal Mesencephalic Tissue in a Patient with Parkinson's Disease. New England Journal of Medicine 332, 1118–1124.

Kordower, J.H., Chu, Y., Hauser, R.A., Olanow, C.W., and Freeman, T.B. (2008). Transplanted dopaminergic neurons develop PD pathologic changes: A second case report. Movement Disorders 23, 2303–2306.

Lau, A., So, R.W.L., Lau, H.H.C., Sang, J.C., Ruiz-Riquelme, A., Fleck, S.C., Stuart, E., Menon, S., Visanji, N.P., Meisl, G., et al. (2020). α-Synuclein strains target distinct brain regions and cell types. Nature Neuroscience 23, 21–31.

Li, B., Ge, P., Murray, K.A., Sheth, P., Zhang, M., Nair, G., Sawaya, M.R., Shin, W.S., Boyer,

D.R., Ye, S., et al. (2018a). Cryo-EM of full-length α-synuclein reveals fibril polymorphs with a common structural kernel. Nat Commun 9, 3609.

Li, J.-Y., Englund, E., Holton, J.L., Soulet, D., Hagell, P., Lees, A.J., Lashley, T., Quinn, N.P., Rehncrona, S., Björklund, A., et al. (2008). Lewy bodies in grafted neurons in subjects with Parkinson's disease suggest host-to-graft disease propagation. Nat Med 14, 501–503.

Li, Y., Zhao, C., Luo, F., Liu, Z., Gui, X., Luo, Z., Zhang, X., Li, D., Liu, C., and Li, X. (2018b). Amyloid fibril structure of α-synuclein determined by cryo-electron microscopy. Cell Res 28, 897–903.

Lo Conte, L., Ailey, B., Hubbard, T.J.P., Brenner, S.E., Murzin, A.G., and Chothia, C. (2000). SCOP: a Structural Classification of Proteins database. Nucleic Acids Res 28, 257–259.

Luk, K.C., Kehm, V.M., Zhang, B., O'Brien, P., Trojanowski, J.Q., and Lee, V.M.Y. (2012). Intracerebral inoculation of pathological α-synuclein initiates a rapidly progressive neurodegenerative α-synucleinopathy in mice. J Exp Med 209, 975–986.

Martin, J.B. (1999). Molecular Basis of the Neurodegenerative Disorders. The New England Journal of Medicine 11.

Mougenot, A.-L., Nicot, S., Bencsik, A., Morignat, E., Verchère, J., Lakhdar, L., Legastelois, S., and Baron, T. (2012). Prion-like acceleration of a synucleinopathy in a transgenic mouse model. Neurobiology of Aging 33, 2225–2228.

Najibi, S.M., Maadooliat, M., Zhou, L., Huang, J.Z., and Gao, X. (2017). Protein Structure Classification and Loop Modeling Using Multiple Ramachandran Distributions. Computational and Structural Biotechnology Journal 15, 243–254.

Némethy, G., and Printz, M.P. (1972). The γ Turn, a Possible Folded Conformation of the

Polypeptide Chain. Comparison with the β Turn. Macromolecules 5, 755–758.

Okun, M.S. (2012). Deep-brain stimulation for Parkinson's disease. N Engl J Med 367, 1529–1538.

Orengo, C., Michie, A., Jones, S., Jones, D., Swindells, M., and Thornton, J. (1997). CATH – a hierarchic classification of protein domain structures. Structure 5, 1093–1109.

Pan, K.-M., Baldwin, M., Nguyen, J., Gasset, M., Mehlhorn, I., Huang, Z., Fletterick, R.J., Cohenu, F.E., and Prusiner, S.B. (1993). Conversion of a-helices into ,f-sheets features in the formation of the scrapie prion proteins. Proc. Natl. Acad. Sci. USA 5.

Papp, M.I., Kahn, J.E., and Lantos, P.L. (1989). Glial cytoplasmic inclusions in the CNS of patients with multiple system atrophy (striatonigral degeneration, olivopontocerebellar atrophy and Shy-Drager syndrome). Journal of the Neurological Sciences 94, 79–100.

Parkinson, J. (2002). An Essay on the Shaking Palsy. J Neuropsychiatry Clin Neurosci 14.

Pawar, A.P., DuBay, K.F., Zurdo, J., Chiti, F., Vendruscolo, M., and Dobson, C.M. (2005). Prediction of "Aggregation-prone" and "Aggregation-susceptible" Regions in Proteins Associated with Neurodegenerative Diseases. Journal of Molecular Biology 350, 379–392.

Peng, C., Gathagan, R.J., Covell, D.J., Medellin, C., Stieber, A., Robinson, J.L., Zhang, B., Pitkin, R.M., Olufemi, M.F., Luk, K.C., et al. (2018). Cellular milieu imparts distinct pathological α-synuclein strains in α-synucleinopathies. Nature 557, 558–563.

Polymeropoulos, M.H., Lavedan, C., Leroy, E., Ide, S.E., Dehejia, A., Dutra, A., Pike, B., Root, H., Rubenstein, J., Boyer, R., et al. (1997). Mutation in the alpha-synuclein gene identified in families with Parkinson's disease. Science 276, 2045–2047.

Prusiner, S.B. (1982). Novel proteinaceous infectious particles cause scrapie. Science 216,

136–144.

Prusiner, S.B., Woerman, A.L., Mordes, D.A., Watts, J.C., Rampersaud, R., Berry, D.B., Patel, S., Oehler, A., Lowe, J.K., Kravitz, S.N., et al. (2015). Evidence for α-synuclein prions causing multiple system atrophy in humans with parkinsonism. Proc Natl Acad Sci USA 112, E5308–E5317.

Ramachandran, G.N., Ramakrishnan, C., and Sasisekharan, V. (1963). Stereochemistry of polypeptide chain configurations. Journal of Molecular Biology 7, 95–99.

Richardson, J.S. (1981). The anatomy and taxonomy of protein structure. Adv Protein Chem 34, 167–339.

Rodriguez, J.A., Ivanova, M.I., Sawaya, M.R., Cascio, D., Reyes, F.E., Shi, D., Sangwan, S., Guenther, E.L., Johnson, L.M., Zhang, M., et al. (2015). Structure of the toxic core of α-synuclein from invisible crystals. Nature 525, 486–490.

Schweighauser, M., Shi, Y., Tarutani, A., Kametani, F., Murzin, A.G., Ghetti, B., Matsubara, T., Tomita, T., Ando, T., Hasegawa, K., et al. (2020). Structures of α-synuclein filaments from multiple system atrophy. Nature.

Shahnawaz, M., Mukherjee, A., Pritzkow, S., Mendez, N., Rabadia, P., Liu, X., Hu, B., Schmeichel, A., Singer, W., Wu, G., et al. (2020). Discriminating α-synuclein strains in Parkinson's disease and multiple system atrophy. Nature 578, 273–277.

Shy, G.M., and Drager, G.A. (1960). A Neurological Syndrome Associated with Orthostatic Hypotension: A Clinical-Pathologic Study. A.M.A. Archives of Neurology 2, 511–527.

Spillantini, M. [Grazia, Crowther, R. [Anthony, Jakes, R., Cairns, N.J., Lantos, P.L., and Goedert,

M. (1998a). Filamentous α-synuclein inclusions link multiple system atrophy with

Parkinson's disease and dementia with Lewy bodies. Neuroscience Letters 251, 205–208.

Spillantini, M.G., Crowther, R.A., Jakes, R., Hasegawa, M., and Goedert, M. (1998b). α-Synuclein in filamentous inclusions of Lewy bodies from Parkinson's disease and dementia with Lewy bodies. Proceedings of the National Academy of Sciences 95, 6469–6473.

Stefanis, L. (2012). α-Synuclein in Parkinson's Disease. Cold Spring Harb Perspect Med 2.

Strohäker, T., Jung, B.C., Liou, S.-H., Fernandez, C.O., Riedel, D., Becker, S., Halliday, G.M., Bennati, M., Kim, W.S., Lee, S.-J., et al. (2019). Structural heterogeneity of α-synuclein fibrils amplified from patient brain extracts. Nat Commun 10, 5535.

Tartaglia, G.G., Pawar, A.P., Campioni, S., Dobson, C.M., Chiti, F., and Vendruscolo, M. (2008). Prediction of Aggregation-Prone Regions in Structured Proteins. Journal of Molecular Biology 380, 425–436.

Touw, W.G., Baakman, C., Black, J., te Beek, T.A.H., Krieger, E., Joosten, R.P., and Vriend, G. (2015). A series of PDB-related databanks for everyday needs. Nucleic Acids Res 43, D364–D368.

Tuttle, M.D., Comellas, G., Nieuwkoop, A.J., Covell, D.J., Berthold, D.A., Kloepper, K.D., Courtney, J.M., Kim, J.K., Barclay, A.M., Kendall, A., et al. (2016). Solid-state NMR structure of a pathogenic fibril of full-length human α-synuclein. Nat Struct Mol Biol 23, 409–415.

Ulmer, T.S., Bax, A., Cole, N.B., and Nussbaum, R.L. (2005). Structure and dynamics of micelle-bound human alpha-synuclein. J Biol Chem 280, 9595–9603.

Van der Perren, A., Gelders, G., Fenyi, A., Bousset, L., Brito, F., Peelaerts, W., Van den Haute,

C., Gentleman, S., Melki, R., and Baekelandt, V. (2020). The structural differences between patient-derived α-synuclein strains dictate characteristics of Parkinson's disease, multiple system atrophy and dementia with Lewy bodies. Acta Neuropathol.

Venkatachalam, C.M. (1968). Stereochemical criteria for polypeptides and proteins. V. Conformation of a system of three linked peptide units. Biopolymers 6, 1425–1436.

Watts, J.C., Giles, K., Oehler, A., Middleton, L., Dexter, D.T., Gentleman, S.M., DeArmond, S.J., and Prusiner, S.B. (2013). Transmission of multiple system atrophy prions to transgenic mice. Proceedings of the National Academy of Sciences 110, 19555–19560.

Woerman, A.L., Stöhr, J., Aoyagi, A., Rampersaud, R., Krejciova, Z., Watts, J.C., Ohyama, T., Patel, S., Widjaja, K., Oehler, A., et al. (2015). Propagation of prions causing synucleinopathies in cultured cells. Proc Natl Acad Sci USA 112, E4949–E4958.

Woerman, A.L., Kazmi, S.A., Patel, S., Freyman, Y., Oehler, A., Aoyagi, A., Mordes, D.A., Halliday, G.M., Middleton, L.T., Gentleman, S.M., et al. (2018a). MSA prions exhibit remarkable stability and resistance to inactivation. Acta Neuropathol 135, 49–63.

Woerman, A.L., Kazmi, S.A., Patel, S., Aoyagi, A., Oehler, A., Widjaja, K., Mordes, D.A., Olson, S.H., and Prusiner, S.B. (2018b). Familial Parkinson's point mutation abolishes multiple system atrophy prion replication. Proc Natl Acad Sci USA 115, 409–414.

Zambrano, R., Jamroz, M., Szczasiuk, A., Pujols, J., Kmiecik, S., and Ventura, S. (2015). AGGRESCAN3D (A3D): server for prediction of aggregation properties of protein structures. Nucleic Acids Res 43, W306–W313.

Zarranz, J.J., Alegre, J., Gómez- Esteban, J.C., Lezcano, E., Ros, R., Ampuero, I., Vidal, L., Hoenicka, J., Rodriguez, O., Atarés, B., et al. (2004). The new mutation, E46K, of α-synuclein causes parkinson and Lewy body dementia. Annals of Neurology 55,

164–173.